# CHARACTERISTICS OF BGO SCINTILLATION DETECTOR IN GAMMA RAY MEASUREMENTS

*A Thesis submitted in partial fulfillment of the requirements for the award of degree of*

**Master of Science**

**In**

**Physics**


Submitted by

Vrinda Thareja

Roll No. 301504038

Under the supervision of

**Dr. Manoj K. Sharma**
Professor and Head

**Dr. Sunil Devi**
Assistant professor

School of Physics and Materials Science (SPMS)

Thapar University, Patiala



School of Physics and Materials Science (SPMS)

Thapar University, Patiala

Patiala-147004, INDIA


July- 2017

*This work is dedicated to my family, friends and teachers.*

*Above all, in fear of the lord.*

# CERTIFICATE

I hereby certify that the work presented in this thesis entitled "Characteristics of BGO scintillation detector in gamma ray measurements" submitted in partial fulfillment of the requirements for the award of degree of Master of Science in physics at Thapar University, Patiala, is an authentic record of my own work carried out under the supervision of Dr. Manoj Kumar Sharma, Professor and Head of School of Physics and Material Science and Dr. Sunil Devi, Assistant Professor, SPMS, Thapar University, Patiala. I have worked at Thapar University or elsewhere, is explicitly acknowledged in the dissertation. Works of other authors cited in this dissertation have been duly acknowledged under reference section of this thesis.

Vrinda

Date: 01/08/2017

Vrinda Thareja

This is to certify that the above statement made by the candidate is correct and true to best of my knowledge.

Dr. Manoj Kumar Sharma
Professor and Head (SPMS)
Thapar University, Patiala

Sunil

Dr. Sunil Devi
Assistant professor (SPMS)
Thapar University, Patiala

# ACKNOWLEDGEMENT

I would like to avail the opportunity to express my most sincere appreciation and deep gratitude to all those people who in a way or other have contributed positively in completion of this dissertation.

First and foremost, I would like to thank God for giving me the strength, knowledge, ability and opportunity to undertake this study and to persevere and complete it satisfactorily. Without his blessings, this achievement would not have been possible.

In my journey towards the degree, I express my sincere regards to my supervisors **Dr. Manoj K. Sharma**, Professor and Head, School of Physics and Material science, Thapar University, and **Dr. Sunil Devi**, Assistant Professor, Thapar University for their inspiring guidance, valuable suggestions, and constant encouragement throughout my work. I am grateful for the experience and diverse opportunity I was given while working with them. Their timely approach and discussions have proved greatly valuable in systematic completion of this work. The knowledge, skills and thoughtfulness that they have imparted will be cherished forever.

My sincere thanks goes to **R. Mathiyarasu** , Scientist 'G', Radiological Safety Division and **Dr. M. Manohari** , Scientist 'D', Radiological Safety Division, Indira Gandhi Centre for Atomic Research, Kalpakkam who provided me an opportunity to join them as intern and who gave access to the laboratory for research facilities. Without their precious support it would not be possible to complete this thesis.

With special mention to Inigo Valan Isaiarasu, Research Scholar, Department of nuclear Physics, Madras University, Chennai, a good friend, for providing me with insightful discussions about the research. His invaluable advice and feedback on my work has been a great support throughout.

I am grateful to my family who have always supported, assisted and encouraged me in achieving my goals.

In my long list of people I cannot forget the cooperation of my friends especially Mehak Sharma, Shivangi Gupta, Anurag Yadav and Ajay Mohan who made my day to day life inside and outside the lab joyous and smooth.

**Vrinda Thareja**

# ABSTRACT

Gamma ray spectroscopy is an analytical approach used to quantify the energy distribution of gamma rays emitted from radioactive sources. This technique can be used for various purposes such as research, health, radioisotope use and astrophysics etc. Radioactive sources emit gamma rays of different energies and intensities. In this work, gamma ray sources $Cs^{137}$, $Mn^{54}$, $Na^{22}$ and $Co^{60}$ are used for studying the interaction of the gamma radiations with the scintillation detector, Bismuth Germanate (BGO) and Sodium Iodide NaI(Tl)). Energy calibration, efficiency calculations and validation of energy calibrations is done for the experimentally measured data. To study the detector performance, a quantitative comparison between BGO and NaI(Tl) detector is established on the basis of energy resolution.

Theoretically, the main purpose here is to obtain gamma ray spectra by means of a scintillation detector (BGO) by applying Monte Carlo simulation method using the MCNP5 code. The MCNP is a software package, used to simulate statistical processes which allows generating random numbers and the result is taken as an average of numbers observed. The MCNP5 program in general, allows the simulation of the following physical processes: photo-electric effect, Compton Effect, electron positron pair generation and processes involving interaction of charged particles with matter. The gamma rays recorded by the detector are converted into electrical pulses and the gamma ray spectra are acquired. The distance between source and detector and thickness of the detector surface are taken as variable parameters during the acquisition of gamma ray spectra in simulation process.

The efficiency for a specific geometry of BGO based gamma spectrometer is estimated experimentally and validated theoretically by comparing the results of the two approaches.

# PREFACE

This thesis is focused on the methodology involved in estimating the efficiency value for a specific geometry of gamma spectrometer (BGO) and to study the detector performance on the basis of energy resolution, a comparison is carried out between BGO and NaI(Tl) detectors. The results presented in this thesis concern the operational properties of BGO and NaI(Tl) detectors.

The main objectives of this dissertation are to understand the:

- Procedure involved in estimating the efficiency for BGO gamma ray spectrometer.
- Comparison between detectors on the basis of energy resolution.
- Spectrum analysis of various radioactive sources ($Co^{60}$, $Na^{22}$, $Cs^{137}$, $Ba^{133}$, $Mn^{54}$).
- Calibration process of scintillation spectrometer using known sources and use it to validate energy calibration.
- Modelling of BGO Detector using MCNP simulation.
- Relative comparison between simulation and experimental results.

**Chapter 1** gives a brief introduction about the concept of gamma rays and their interaction with matter. It also discusses about radiation spectroscopy with main focus on scintillation detectors used in gamma ray spectroscopy.

**Chapter 2** explains the methodology used in energy calibration and efficiency calculation. This chapter presents a comparison plot between BGO and NaI(Tl) detectors on the basis of their energy resolutions.

**Chapter 3** gives the MCNP features, a theoretical approach used in calculating the efficiency of BGO detector. The simulated spectrum of radioactive sources with their analysis has been included. In addition, the source code used to model the BGO detector is also presented.

The results of experimental measurements and simulations along with the discussion are briefly summarized in **chapter 4.**

# LIST OF FIGURES

## Chapter 1



## Chapter 2



## Chapter 3

### Chapter 4



## LIST OF TABLES

### Chapter 1



### Chapter 2



### Chapter 3



### Chapter 4

# TABLE OF CONTENTS

# CHAPTER 1

# INTRODUCTION TO RADIATION SPECTROSCOPY

This chapter discusses about the theory involved in the study of gamma ray interactions with matter. Section 1.1 introduces the concept of gamma rays and the sources of gamma-ray emission. Section 1.2 discusses about the three major types of gamma-ray interactions with matter. Section 1.3 gives the brief description of the detectors used in gamma ray spectroscopy. Section 1.4 discusses about the scintillator detector principles and the operational mechanism of the detector. Section 1.5 gives the review of various inorganic scintillators out of which BGO and NaI(Tl) is of much importance.

## 1.1 Gamma rays (sources of gamma emission):

Gamma rays, (or gamma radiations) are the high frequency electromagnetic radiations and consist of high energy photons. Gamma radiations are produced by the process of gamma decay of an atomic nucleus from a high unstable energy state to lower stable energy state.
Gamma rays are emitted through various processes:

### 1.1.1 Emission of gamma rays by excited nucleus

Gamma radiation is emitted when a nucleus decays to lower lying nuclear levels. In the decay of the parent radionuclide, the excited nuclear states are created [1] .The decay scheme of $Co^{60}$ is shown in Fig 2.8. In $Co^{60}$, a process of $\beta^-$ decay leads to the excited states in daughter nucleus and de-excitation leads to $\gamma$ ray photon.

$$^{60}_{27}Co \rightarrow {}^{60}_{28}Ni^{*} + \beta^{-} + \bar{\nu} \qquad (1.1)$$

### 1.1.2 Annihilation Reaction

When the parent nucleus undergoes $\beta^+$ decay, the positron emitted in the primary decay process combine with electron in the absorbing material resulting in annihilation. The original electron and positron disappear and are replaced by two oppositely directed electromagnetic photons of energy 0.511 MeV each known as annihilation radiation [10].

### 1.1.3 Gamma emission following nuclear reactions

In such a nuclear transformation, collision of a particle or a photon with a nucleus results in the formation of product radionuclide with an emission of particle or gamma ray photon [2].

$$ {}^{4}_{2}\alpha + {}^{9}_{4}Be \rightarrow {}^{12}_{6}C^{*} + {}^{1}_{0}n \qquad (1.2) $$

Here, in equation (1.2), product nucleus $^{12}$C formed is in the excited state, its decay gives rise to gamma ray photon of 4.44 MeV energy [1].

## 1.2 Gamma ray interactions with matter

Gamma rays, unlike $\alpha$ and β rays are uncharged radiations and therefore cannot produce electrical signal within the detector by the mechanism of ionization. Detection of gamma ray depends upon the processes by which it interacts with matter [4]. There are predominantly three major ways by which gamma rays transfer its energy to electrons in the material: (i) photoelectric absorption (ii) Compton scattering and (iii) pair production [2].

### 1.2.1 Photoelectric absorption

In photoelectric absorption, gamma ray transfers its complete energy to electrons in the detector material and then photon disappears. In the process, photoelectron is ejected from bound shells of the atom, with kinetic energy $E_o$ given by,

$$ E_o = E_\gamma - E_b \qquad (1.3) $$

Where, $E_b$ represents the binding energy of bounded photoelectron and $E_\gamma$ represents the energy of incident gamma ray. The probability of occurrence of photoelectric effect depends on the atomic number of absorbing material and energy of incident gamma ray. An approximation to describe the relation between probability of this effect over all gamma ray energies of interest is given by,

$$ \tau \propto \frac{Z^n}{E_\gamma^{3.5}} \qquad (1.4) $$

Where, Z is the atomic number of detector material, value of n ranges from 4 to 5, τ represents the probability of photoelectric absorption per atom over all ranges of $E_\gamma$ of interest and Z [7,9].

### 1.2.2 Compton scattering

In Compton scattering, gamma ray interacts with a free or a weakly bound electron and transfers a fraction of its energy to the recoil electron which scatters off in other direction [6]. The photon is scattered by an angle θ as represented in fig 1.1 [4].

The energy imparted to the recoil electron is given by,

$$E_e = E_\gamma - E_{\gamma'} \qquad (1.5)$$

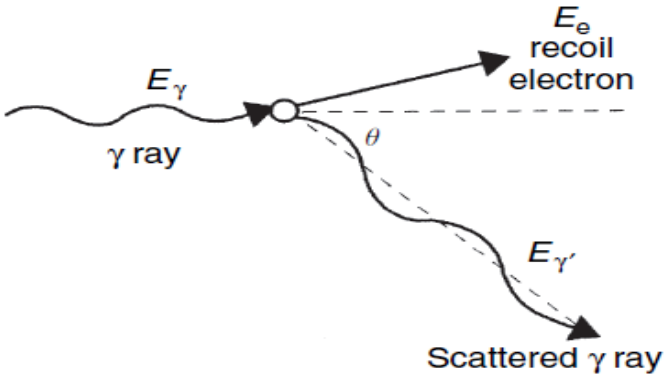


***Fig 1.1.*** *Mechanism of Compton scattering.*

Where, $\mathbf{E_e}$ is the energy of recoil electron, $\mathbf{E_\gamma}$ represents the energy of incident gamma ray, and $\mathbf{E_{\gamma'}}$ represents the energy of scattered gamma ray photon. The energy of the scattered photon in terms of its scattering angle and the energy of the original photon is given as [1]:

$$E_{sc} = \frac{E_\gamma}{1+\frac{E_\gamma}{m_o\ c^2}(1-\cos\theta)} \qquad (1.6)$$

The probability of occurrence of Compton scattering process ($\sigma_C$) is directly proportional to the atomic number Z of the absorbing material and varies inversely with the energy E of the incident photon. The expression given by [7]

$$\sigma_C \propto \frac{Z}{E} \qquad (1.7)$$

### 1.2.3 Pair Production

In pair production process, an electron and a positron is created due to strong field effects experienced by photon from the nucleus of absorbing material. The electron and positron are

created in pairs and total disappearance of gamma ray is observed. A schematic of pair production is shown in Fig. 1.2. [4]

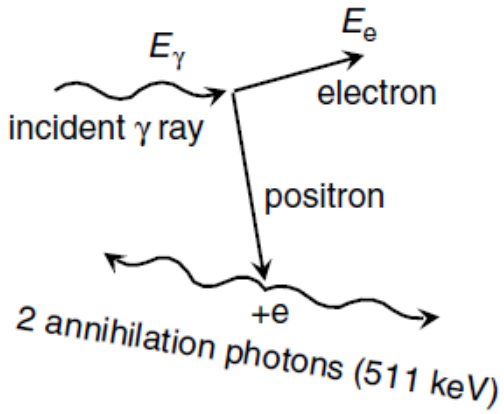


***Fig 1.2.*** *Mechanism of pair production process.*

This process occurs only if the gamma ray enters the material with energy greater than twice the rest mass energy of the electron (1.022 MeV), which is required to create electron-positron pair. Any excess energy above 1.022 MeV is shared between electron-positron pair [1].

$$E_\gamma = E_{e^+} + E_{e^-} + 1.022 \quad (1.8)$$

The probability of pair production process ($\sigma_{pp}$) is predominant at high energy gamma rays and increases with the increase in atomic number, the approximation given as, [7,9]

$$\sigma pp \propto (E\text{-}1.02)^2 Z^2 \quad (1.9)$$

## 1.3 Gamma ray detectors

The major concern in the detection of gamma rays depends upon the production of charged particles which can be collected to produce an electrical signal within a detector. The ways in which gamma rays transfer their energy to the electrons can be explained through the mechanisms as discussed in section 1.2. The electrons form the basis of a detector signal. The desirable features of materials suitable for constructing gamma ray detectors should be such that it has good efficiency, good energy resolution, short decay time, reasonable cost and size [8]. The two type of detectors are particularly used in gamma ray spectroscopy are:

- Semiconductor detectors such as HPGe
- Scintillation detectors – NaI(Tl) , BGO , $LaBr_3$

There are circumstances where good energy resolution is not required and space restrictions prevent the use of semiconductor detectors. In those cases, scintillation materials that have found particular application in gamma ray measurements are all inorganic crystals: Sodium Iodide (NaI), Cesium Iodide (CsI), Calcium Fluoride ($CaF_2$), Bismuth Germanate (BGO) [4] etc.

## 1.4 Scintillation detector

A scintillator is a material that exhibits the property of radiance when excited by ionizing radiation. Luminescent materials, when struck by energetic particles (γ rays), re-emit the energy which is absorbed in the form of light [12].The energy of incoming particles are converted into photons of much lower energy in the visible range that can be detected with photomultipliers (PMT) or photodiodes. The details of the different components of a typical scintillation detector are shown in Fig 1.3 [1].

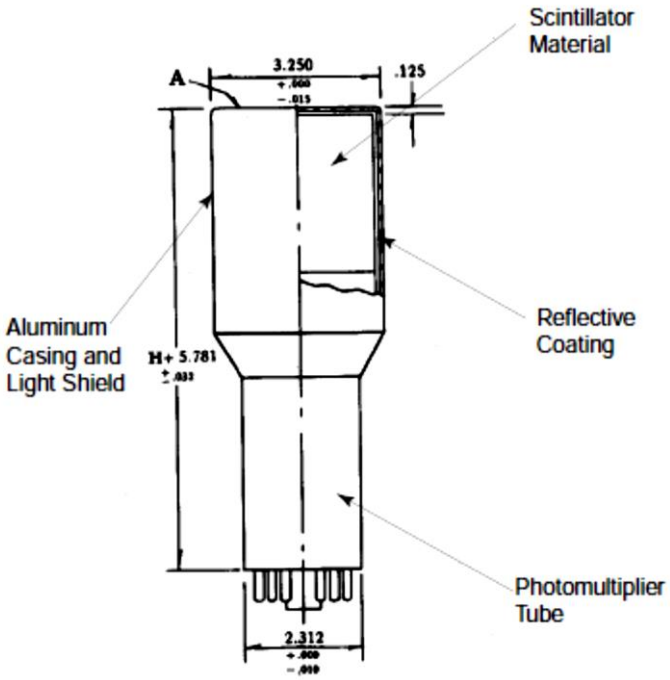


***Fig 1.3****. Components of a scintillator detector.*

### 1.4.1 Operational mechanism in scintillator

As the gamma ray passes through the scintillator medium, it undergoes interaction in the lattice through the processes discussed in section 1.2, which further creates energetic electrons. The atoms and molecules of the scintillator material get excited causing light to be emitted. This

light is further transmitted to the photomultiplier tube through optical coupling system where photons have a very high probability of undergoing photoelectric effect in the photocathode, thereby creating a weak current of photoelectrons. The detector gives signal in the form of current. The weak signal is further amplified using amplifier, where photoelectrons liberated are accelerated by a strong electric field towards the dynode, maintained at positive polarity relative to photocathode. The dynode ejects more electrons than incident ones, causing increase in electron flux. The process continues for the series of dynodes, resulting in signal amplification as shown in Fig 1.4. The current signal is analyzed by using an ADC (analog to digital converter) for each PMT. It converts the analog signal coming from the amplifier to equivalent digital form and assigns a digital number representing the amplitude of the signal. From ADC the signal goes to MCA or multichannel analyzer. A multichannel analyzer after sorting out the incoming pulse, keeps the count of the number at each height in a multichannel memory. The MCA is connected to a computer which shows the energy spectrum of the gamma rays. The spectrum can further be analyzed to find the energy resolution and efficiency for each energy peak in the spectrum. The conversion of signal to channel number is done by MCA. So the obtained spectrum shows counts vs channels. The spectrum is then calibrated by linear calibration to get the counts vs energy spectrum [5].

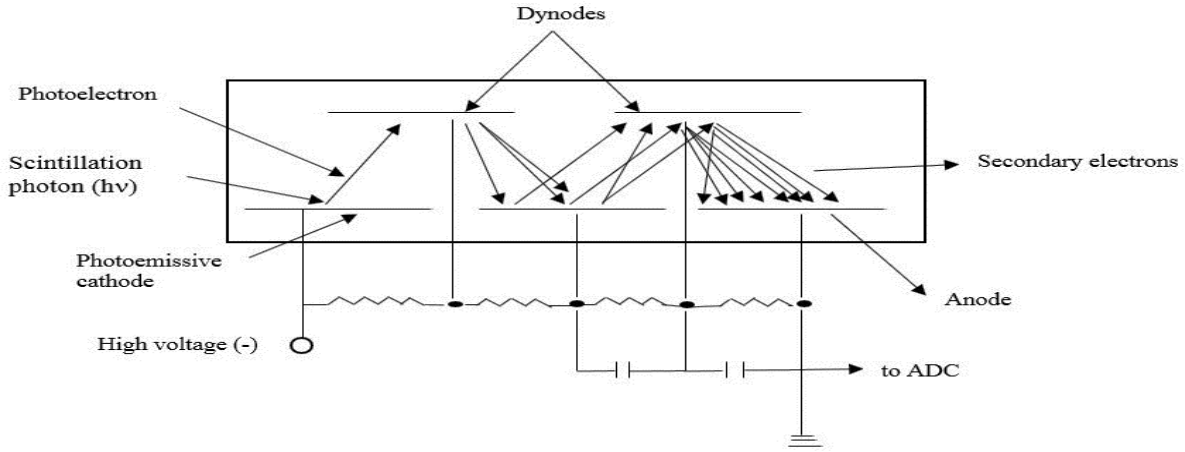


***Fig 1.4.*** *Amplification of electrons in a scintillator detector by PMT.*

### 1.4.2 General considerations in gamma ray measurements

Any detection system, can be defined in terms of four response characteristics:

**(i) Intrinsic efficiency:** proportion of actually detected emissions that reach the detector.

**(ii) Total efficiency:** ratio of the detected emission to the source emission.

**(iii) Geometry**: fraction of the total solid angle covered by the detector due to source emissions.

**(iv) Resolution**: ability of a detector to differentiate between two gamma rays of close by energies.

## 1.5 Review of scintillator detectors used in gamma ray measurements

Scintillation and semiconductor detectors are the two types of solid state detectors, commonly used in gamma ray measurements. A number of materials are used for scintillation detection for example inorganic crystals, glass materials etc. BGO and NaI(Tl) are of prime concern in this thesis.

### 1.5.1 BGO Detector

BGO is an inorganic chemical compound of bismuth, germanium and oxygen, chemical formula given by $Bi_4(GeO_4)_3$. The light output of BGO is low in comparison to NaI(Tl). The density of BGO is approximately 2.5 times that of NaI(Tl) which gives it a high stopping power and makes it ideal for active shielding systems [4]. It is characterized by short decay constant. A typical BGO detector is shown in figure 1.5.

***Fig 1.5.*** *BGO detector*.

- **Scintillation mechanism in BGO**

BGO is used without activator. There is a large shift between the optical and emission spectra of $Bi^{3+}$ states [4]. BGO crystal is transparent to its own emission and relatively little self-absorption takes place. BGO is non-hygroscopic and inert and hence need not be encapsulated. Properties of a typical BGO detector are given in Table 1.1 [4,11].

| Properties of BGO | |
|---|---|
| Density | 7.13 g/cc |
| Light output relative to NaI(Tl) | 12-14% |
| Wavelength of Maximum emission | 480 nm |
| Decay constant | 0.3μs |
| Hygroscopic | No |

***Table 1.1.*** *Properties of BGO detector.*

### 1.5.2 NaI(Tl) detector

Thallium activated sodium iodide, the most commonly used scintillation material which produces better luminescence compared to other spectroscopic scintillators with good efficiency. NaI(TI) has a high gamma-ray absorption coefficient and provides the greatest light output of all of the inorganic scintillators, it also has the best energy resolution. It is hygroscopic and must be enclosed at all times.

- **Scintillation mechanism in NaI(Tl)**

The electronic orbitals of sodium and iodide atoms combine to form a valence band and a conduction band of molecular orbitals. The thallium impurity create electron orbitals between the conduction and valence band called activation centers. In the ground state, the conduction band and the excited energy levels of the activation centers are empty and the valence band and the ground state level of each activation center are filled with electrons. Thus, in the absence of radiation, there is no electron movement. Incoming gamma ray interacts with the crystal and creates many secondary electrons with high kinetic energy. These electrons cause ionization and excitation as they move, creating more electrons which causes excitation of electrons from valence to conduction band. The electrons that get into conduction band are free to move, but will not fall directly to valence band and so they occupy lowest energy levels available to them which are excited states of activator sites.

In the same way, holes will allow electrons in the valence band to move and eventually will be filled by electrons from activation centers, leaving vacancies in the activation center ground

state level. Since the electron cannot undergo transition from excited state to ground state in activation center, so electron drops down and fills the hole with the excess energy released in the form of light. Properties of NaI(Tl) are listed in table 1.2. [4,11]

| Properties of NaI | |
|---|---|
| Density | 3.67 g/cc |
| Wavelength of Maximum emission | 415 nm |
| Activator | Thallium (Tl) |
| Decay constant | 0.2 μs |
| Hygroscopic | Yes |

***Table 1.2.*** *Properties of NaI(Tl) detector.*

## References:


[1] G.F. Knoll. Radiation Detection and Measurement. John Willey and Sons, 1989.

[2] J. Bryan. Introduction to Nuclear Science. CRC Press, 2009.

[3] S. N. Ahmed. Physics and Engineering of Radiation Detection. Elsevier, 2007.

[4] Gilmore, Gordon. Practical gamma-ray spectroscopy. John Wiley & Sons, 2011.

[5] Brian M. Tissue, 1996, http://elchem.kaist.ac.kr/vt/chem-ed/optics/detector/pmt.htm

[6] Nelson, G., and D. Reilly. "Gamma-ray interactions with matter." Passive nondestructive analysis of nuclear materials (1991): 33-36.

[7] Ragheb, M. "Gamma Rays Interactions with Matter." Nuclear, Plasma and Radiation Science. Inventing the Future," https://netfiles. uiuc. edu/mragheb/www (2011).

[8] Moszynski, M. (2003). "Inorganic scintillation detectors in γ-ray spectrometry." Nucl. Instr. Meth. Phys. Res., A, 505, 101–110.

[9] N Reguigui, Gamma Ray Spectrometry practical information manual – CNSTN(2006)

[10] Vlachos, D. S., and T. E. Simos. "PDSW: A program for the calculation of photon energy distribution resulting from radioactive elements in seawater." Computer physics communications 174.5 (2006): 393.

[11] Nestor, O. H., and C. Y. Huang. "Bismuth Germanate: a high-Z gamma-ray and charged particle detector." IEEE Transactions on Nuclear Science 22.1 (1975): 68-71.

[12] Sciarra et al.," Geochemical and radiometric profiles through an active fault in the Sila Massif (Calabria, Italy)", Journal of Geochemical Exploration, 2015.

# CHAPTER 2

# EXPERIMENTAL METHODOLOGY

This chapter gives a broad description about the experimental setup and the methodology used to explain the measurements obtained. Section 2.1 presents the BGO based gamma ray spectrometer setup along with the components and operating parameters involved in the experiment. Section 2.2 discusses about the characteristics of sources used along with their decay scheme. Section 2.3 concerns with the method involved in energy calibration, along with the energy calibration plot and its validation using experimental measurement. Section 2.4 explains the procedure involved in calculating efficiency for BGO detector. Section 2.5 deals with the effect of background radiations. Finally, comparison between BGO and NaI(Tl) detector is drawn on the basis on energy resolution, which is discussed in section 2.6.

## 2.1 Instrumentation – BGO based gamma ray spectrometer

A BGO based gamma ray spectrometry system as shown in fig 2.1 is used to carry out the energy and efficiency measurements in the present work.

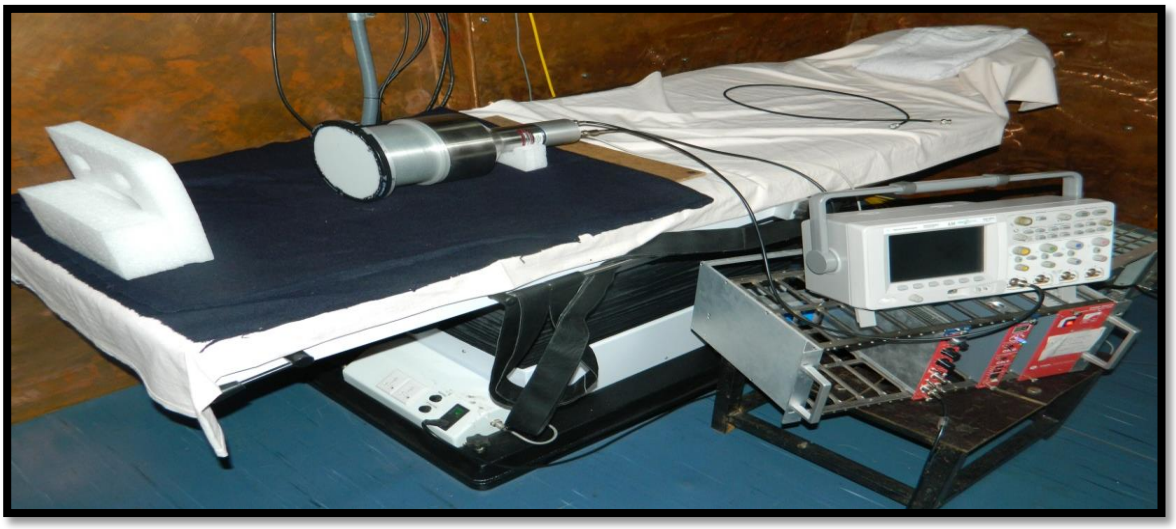

***Fig 2.1**. A BGO based gamma ray spectrometer setup.*

## 2.1.1. Components and operating parameter

The spectrometer consists of a BGO detector, a spectroscopic amplifier, multichannel analyzer (MCA) and a gamma spectral analyzer. The detector bias was kept at 790 V. A positive unipolar output was taken from amplifier by keeping shaping time 1 μs.

The details about detector are as follows:

- formula: $Bi_4Ge_3O_{12}$
- diameter – 12.7 cm
- height – 10.2 cm
- aluminum cap – 0.5 cm
- opening window size – 3cm x 3 cm

A typical block diagram of the BGO detector assembly is shown in fig 2.2, [3]

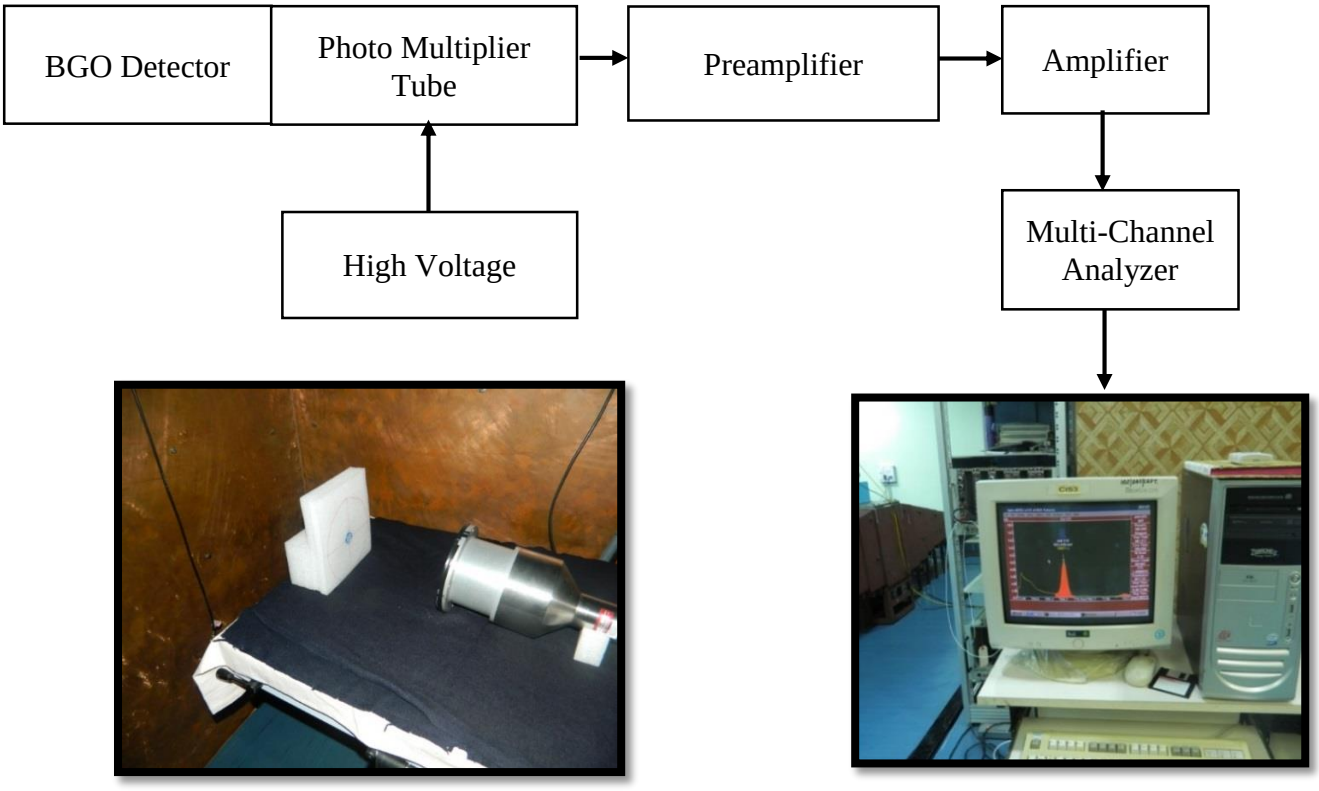


BGO detector with source placed at 27.2 cm from the detector

Gamma spectral analyzer (PC based)

***Fig 2.2**. Block diagram for BGO detector assembly.*

## 2.2 Characteristics of sources used in the experiment

### 2.2.1 Cesium-137

- Principle decay mode: β decay
- Energy (KeV): 662
- Half-life ($t_{1/2}$): 30 years
- Gamma yield : 0.85
- Fig 2.3 represents decay scheme of $Cs^{137}$ [2,8]

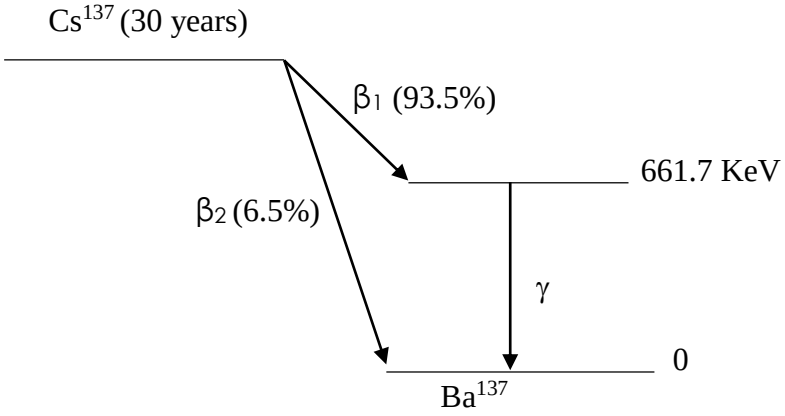


***Fig 2.3**. Decay scheme of $Cs^{137}$*

### 2.2.2 Manganese-54

- Principle decay mode: Electron capture (EC)
- Energy (KeV): 834
- Half-life ($t_{1/2}$): 0.855 years
- Gamma yield : 0.997
- Fig 2.4 represents decay scheme of $Mn^{54}$ [8]

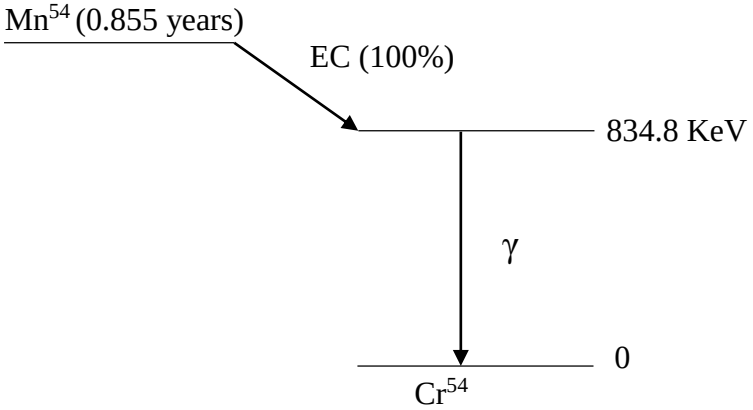


***Fig 2.4**. Decay scheme of $Mn^{54}$*

### 2.2.3 Sodium-22

- Principle decay mode: $\beta^+$ , Electron capture (EC)
- Energy (KeV): 1274
- Half-life ($t_{1/2}$): 2.6 years
- Gamma yield : 0.997
- Fig 2.5 represents decay scheme of $Na^{22}$ [2,8]

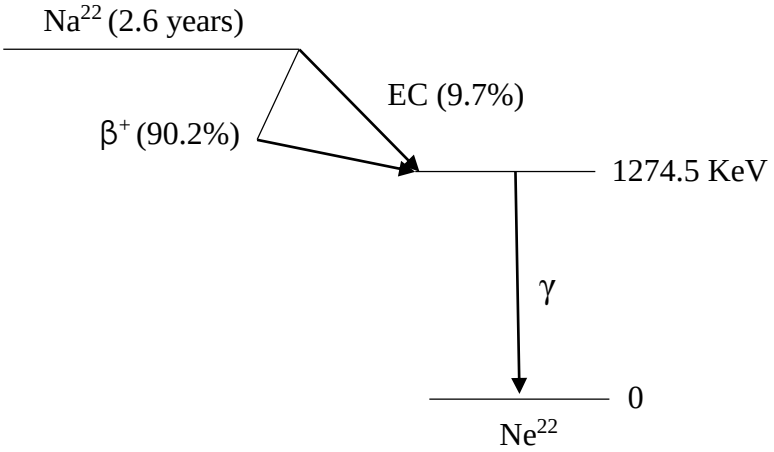


***Fig 2.5.*** *Decay scheme of $Na^{22}$*

### 2.2.4 Cobalt-60

- Principle decay mode: $\beta^-$ decay
- Energy (KeV): 1173, 1332
- Half-life ($t_{1/2}$): 5.27 years
- Gamma yield : 100
- Fig 2.6 represents decay scheme of $Co^{60}$ [2,8]

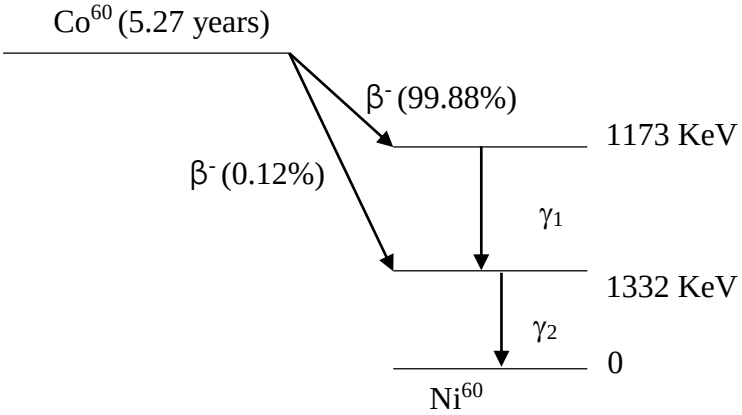


***Fig 2.6****. Decay scheme of $Co^{60}$*

## 2.3 Experimental procedure :

Energy calibration, total efficiency calculation, background measurements and individual spectrum of sources are taken as per the procedure given the operational manual of BGO based gamma ray spectrometer [3], and will be discussed in the following sections.

### 2.3.1 Energy calibration

The purpose of energy calibration is to deduce a relationship between peak channel position in the spectrum and the corresponding gamma ray energy. Energy calibration can be accomplished by measuring the spectrum of gamma rays of known energy and comparing the measured peak channel position with energy. Irrespective of the source used, it is necessary to ensure that the calibration energy spans the entire range over which the spectrometer is to be used. The computer can then search for the peaks, measure the peak position to a fraction of a channel and a relationship between channel number and energy can be derived, in accordance with equation,

$$\text{E } (KeV) = \text{A } (KeV) + \text{B*C (Channels)} \qquad (2.1)$$

Where, A is the intercept, B (KeV/ch) is the gradient of the calibration line and C is the channel number.

Energy calibration is often performed before acquisition of the spectrum as a part of the setting up procedure. By using standard radioactive sources with known gamma ray energies, it can be inferred that the detected gamma ray energies match with the correct channels in computer program. Gamma sources $Am^{241}$ (59.54 KeV), $Na^{22}$ (511 KeV and 1274 KeV) and $Tl^{208}$(2614 KeV) are used for energy calibration. The source is kept at a distance of 27.2 cm distance from the center of detector. Spectrum is acquired for 1000 sec. Peak channel positions versus energy of gamma rays are fitted for obtaining the energy calibration coefficients. A graph between peak channel positions and the corresponding energies is plotted using linear equation 2.1 and is shown in Fig 2.7

$$E(KeV) = a + bX \qquad (2.2)$$

Where, ‘a’ is the intercept, ‘X’ is channel number and ‘b” is slope.

Table 2.1 lists the channel numbers corresponding to different gamma ray energies.

| Sources used | Channel number | Energy ( KeV) |
|---|---|---|
| $Am^{241}$ | 16 | 60 |
| $Na^{22}$ | 168 | 511 |
| $Na^{22}$ | 428 | 1274 |
| $Tl^{208}$ | 883 | 2614 |

***Table 2.1.*** *Energy Calibration Data.*

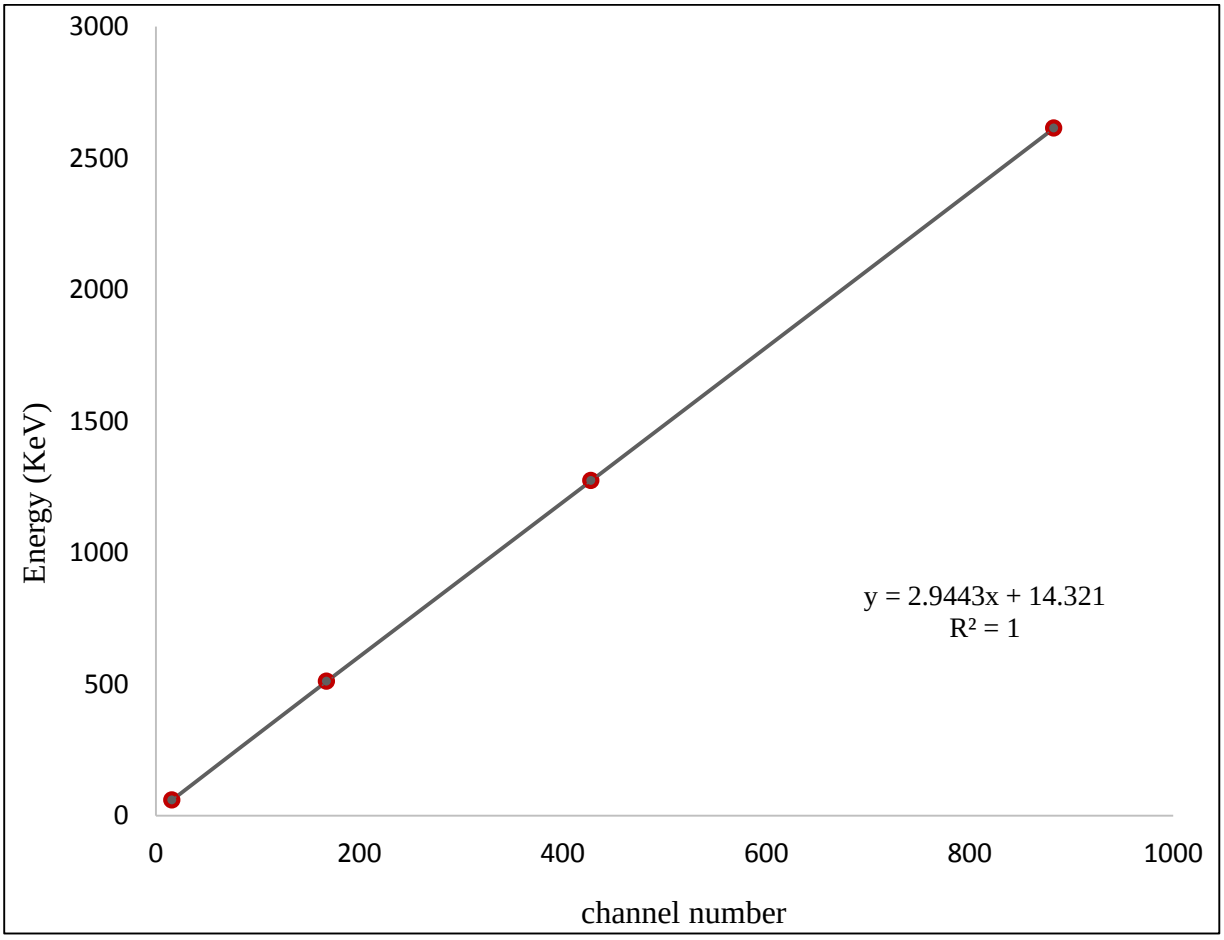


***Fig 2.7.*** *Energy calibration curve.*

The linear fit of energy and channel number data is performed and energy calibration coefficient is calculated which comes out to be 2.9443 KeV/channel. $R^2$ represents the statistical measure of how well, the data points are well approximated on the regression line.

### 2.3.2 Validation of energy calibration using experimental measurement

Energy calibration can be validated by keeping a known gamma ray source in front of detector setup. By using energy calibration coefficients, the gamma ray energy of known isotope can be determined by analyzing channel number and using equation 2.1, energy calibration can be validated. In this work, energy calibration is carried out using BGO as a gamma spectrometer and the energy calibration factor is found to be 2.944 KeV/Channel and the isotope used is Co-57. Peak for this source came at 40 channel number and from the calibration factor, energy determined is 120 KeV. Thus, energy calibration is validated.

## 2.4 Efficiency calculation

The next step is to calculate the total efficiency of the detector which is required to relate the counts in the spectrum to the gamma ray emissions by the source [4]. The efficiency calculation is done for sources $Cs^{137}$, $Mn^{54}$, $Na^{22}$. Spectral parameters such as peak position, FWHM for a standard source such as $Cs^{137}$ is measured. The gamma ray source is kept at a distance of 27.2 cm such that the center of source coincides with the center of detector and spectrum is acquired for specified time, t =1000 seconds. The ROI (region of interest) for the required energy is marked and the gross counts are noted down. After removing the source, background counts have been taken into consideration and net counts which is the subtraction of background counts from the gross counts are noted down.

Count rate which is the division of net counts by counting time is calculated and hence, the efficiency is calculated by dividing the count rate by activity of the source. The calculated efficiency is divided by the yield or abundance of the gamma photons to get efficiency per single photon (cps/photon). The same procedure is repeated to calculate the efficiency values for the other sources [3]. Standard net counts in each ROI is corrected for background.

Net CPS in each ROI is calculated as given below

$$Net\ CPS\ in\ ROI = \frac{Net\ counts\ in\ ROI - Bkg\ counts\ in\ ROI}{Counting\ time(\mathrm{s})} \tag{2.3}$$

Then the efficiency factor, η for that energy ROI is calculated using the formula

$$\text{Efficiency factor}(\eta) = \frac{\text{Net CPS in ROI}}{\text{Activity (Bq)}} \tag{2.4}$$

Efficiency values for the other sources used as per given in the table 2.2:

| Radio-nuclide | Activity (Bq) (as on Jun, 2016) | γ Energy (KeV) | ROI (KeV) | Gamma yield | Net counts | Net cps | Measured Efficiency in cps/photon |
|---|---|---|---|---|---|---|---|
| $^{137}$Cs | 6612 Bq | 662 | 560-760 | 0.85 | 33983 | 56.63 | 1.03E-02 |
| $^{54}$Mn | 797 Bq | 834 | 740-937 | 0.9997 | 27282 | 7.36 | 9.50E-03 |
| $^{22}$Na | 7015 Bq | 1274 | 1130-1414 | 0.9994 | 40693 | 67.82 | 9.65E-03 |

***Table 2.2.*** *List of various sources used for efficiency calculation.*

## 2.5 Background measurements

To study the effect of shielding, background measurements are carried out inside a room which is made of Pre-war steel of dimensions - 200 cm × 200 cm × 190 cm and outside shield room. To suppress background contributions, the shield is with graded shielding arrangement (3mm Pb, 2mm Cd, 1mm Cu). A picture of shield room is shown in fig 2.8.

***Fig 2.8****. Shield room.*

Background radiations are reduced to 1/10th inside the shield room and many of the peaks in the spectrum taken outside shield get vanished as compared to the one taken inside the shield. The recorded spectra of background inside and outside the shield room are shown in Fig 2.9.

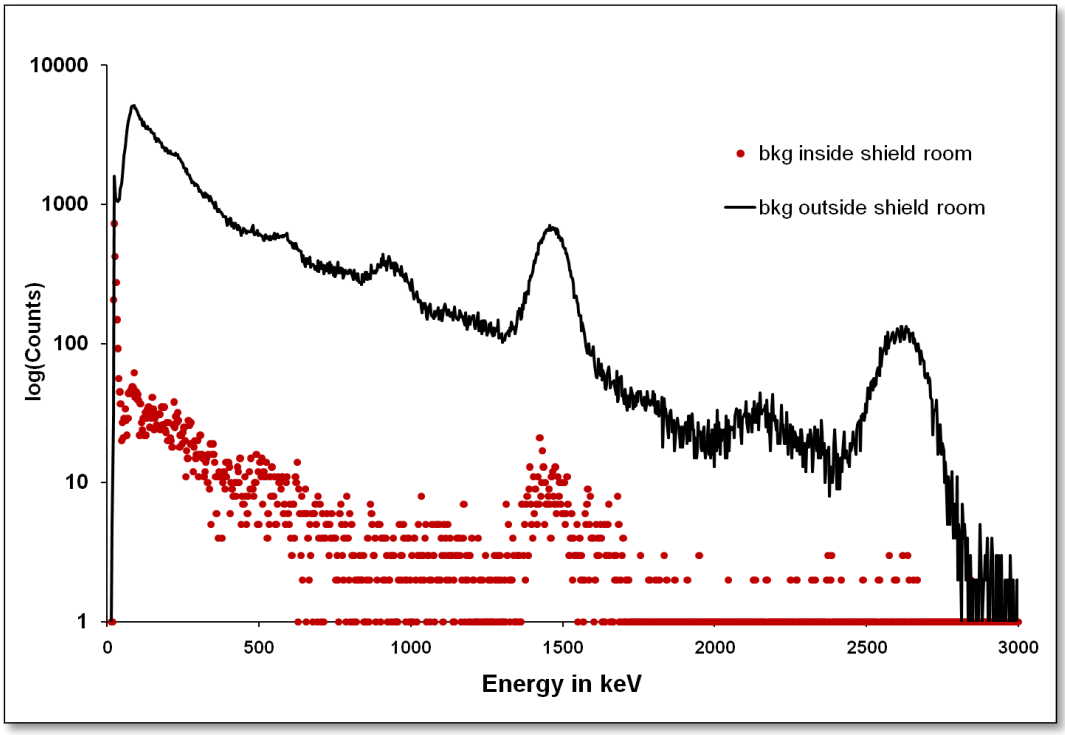


***Fig 2.9***. The recorded background spectra. The solid black line is for background outside the shield room and the red dotted line is for background inside the shield room.

Most significant gamma rays in background are found to be [1,5,6]

- K-40 : 1460 KeV
- Ac-228 : 911 KeV and 968 KeV, 1460 KeV
- Tl-208 : 1620 KeV , 2614 KeV [6]

## 2.6 Energy resolution

The ability of a detector to distinguish between radiations of similar energy is called energy resolution. The energy resolution is a dimensionless quantity and is expressed in fraction (or %). The smaller being the value of resolution, better will be the detection capability to resolve two radiation peaks whose energies lie close to each other. The resolution of a detector is defined

by ratio of FWHM / peak centroid. Where, FWHM is the full width at half maximum of corresponding peak [9].

The table 2.3 and 2.4 represent the energy resolution of the BGO and NaI(Tl) detectors respectively along with the FWHM values.

| Sources | Energy (KeV) | FWHM (KeV) | Resolution (%) |
|---|---|---|---|
| $Cs^{137}$ | 662 | 74.16 | 11.2 |
| $Na^{22}$ | 1274 | 95.91 | 7.5 |
| $Co^{60}$ | 1332 | 95.83 | 7.5 |
| $K^{40}$ | 1460 | 100 | 6.6 |

***Table 2.3.*** *Energy resolution of BGO Detector along with the FWHM values.*

| Sources | Gamma ray energy (exp.) | FWHM (KeV) | Resolution (%) |
|---|---|---|---|
| $Ba^{133}$ | 360.7 | 32.3 | 8.9 |
| $Na^{22}$ | 510.8 | 43.5 | 8.5 |
| $Na^{22}$ | 1280.1 | 71.5 | 5.6 |
| $Cs^{137}$ | 661.6 | 49.4 | 7.5 |
| $Co^{60}$ | 1168 | 67.2 | 5.7 |
| $Co^{60}$ | 1330.4 | 72.5 | 5.4 |

***Table 2.4****. Energy resolution of NaI(Tl) Detector along with the FWHM values.*

Fig 2.10 depicts the comparison between energy resolution of BGO and NaI(Tl) detectors.

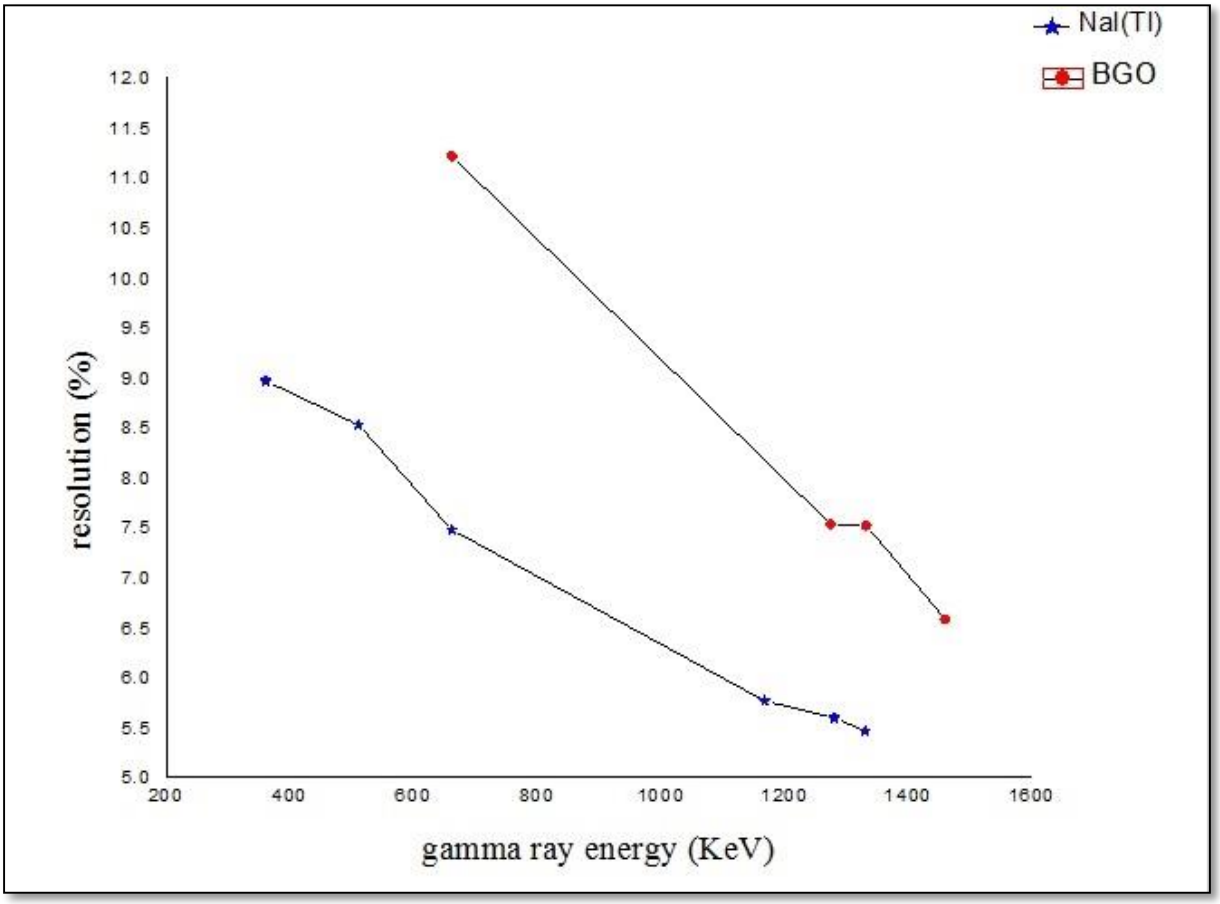


***Fig 2.10**. Energy resolution comparison between BGO and NaI(Tl) detectors.*

### 2.6.1 Inference

At lower energies, in case of $Cs^{137}$ (662 KeV), the energy resolution of NaI(Tl) and BGO are 7.5% and 11.2% respectively. This implies, NaI(Tl) performs better than BGO at low energy range. The energy resolution of both the detector improve significantly for high energy gamma rays and the difference between two detectors resolution becomes less significant. As in general, at the low energies, the resolution of NaI(Tl) is better than BGO [7]. This makes NaI(Tl) a better choice to detect gamma rays at low energies. BGO is fairly better choice for detecting high energy gamma rays as it has better efficiency and its energy resolution is slightly poor as compared to NaI(Tl).

**References:**

[1] G.F. Knoll. Radiation Detection and Measurement. John Willey and Sons, 1989.

[2] Data extracted from National Nuclear Data Center, worldwideweb site.

[3] N Reguigui , Gamma Ray Spectrometry practical information manual – CNSTN(2006)

[4] Lepy, Marie-Christine. "Detection efficiency." IAEA-ALMERA Technical Visit at Laboratoire National Henri Becquerel (2010).

[5] Lemley, J. R., et al. "Confirmatory Measurements for Uranium in Nuclear Weapons by High Resolution Gamma-Ray Spectrometry (HRGS)." Report BNL-66293, Brookhaven National Laboratory, Upton, NY (1999).

[6] Calin, M. R., and A. E. Druker. "The energy and FWHM calibration of a gamma spectrometric system with a HPGe detector on the basis of the background spectrum." Rom. Journ. Phys 56.7-8 (2011): 920-927.

[7] Gierlik, Michał, et al. "Comparative study of large NaI (Tl) and BGO scintillators for the european illicit trafficking countermeasures kit project." IEEE transactions on nuclear science 53.3 (2006): 1737-1743.

[8] Rittersdorf, Ian. "Gamma ray spectroscopy." Nuclear Engineering & Radiological Sciences (2007): 18-20.

[9] Minty, Brian Robert Stuart. "Fundamentals of airborne gamma-ray spectrometry." AGSO Journal of Australian Geology and Geophysics 17 (1997): 45

# CHAPTER 3

# SIMULATION- MONTE CARLO METHOD

This chapter discusses about the methodology involved in theoretical calculations in the framework of Monte Carlo method (MCNP). Section 3.1 gives an introduction of numerical methods with main focus on Monte Carlo method. Section 3.2 discusses about the theoretical part associated with MCNP. Section 3.3 explains MCNP features which will further help in developing the source code to model the detector. Section 3.4 concerns with the programming to model the BGO detector. Section 3.5 deals with the importance of Gaussian energy parameters. Section 3.6 depicts the simulated spectrum of sources used in the experimental measurements. Effect of varying thickness of the detector, and source position from the detector on the total efficiency has been discussed in section 3.7

## 3.1 Introduction

Numerical models are used to check and verify the effect of gamma-ray interaction in the detectors. Simulation is the imitation of the operation of a real world process or system over time. Monte Carlo enables simulation of any process that is influenced by random factors and cannot be modelled using deterministic method [6]. MCNP is a theoretical approach used to simulate statistical processes such as the interaction of nuclear particles with matter.

## 3.2 Theoretical background

The Monte Carlo Neural Particle Code (MCNP), a software toolkit which is developed and maintained by Los Alamos National Laboratory, is the internationally recognized code for analyzing the transport of neutrons and gamma rays by the Monte Carlo method [1]. MCNP is a generic approach that can be used in various modes such as transport of electrons, neutrons and photon transport etc. Here we have used MCNP5, Monte Carlo Neutral Particle code. MCNP uses random number to track each particle and records the average behavior. Numbers between 0 and 1 are distributed uniformly and a random selection is made to determine the kind of interaction taking place, based on the probabilities governing the processes [4]. An input file is created by the user that is read by MCNP. Information regarding geometry specification,

material description, desired tally, and variance reduction techniques is contained in that file [5]. Ultimate aim of this simulation is to track each individual photon until one of the two cases occur:

(i) The gamma photon deposits all its energy in the modelled detector by various process like photoelectric absorption, Compton scattering, pair production or other processes [8].

(ii) The gamma photon escapes from the modelled detector or the outer canning material around the detector surface.

## 3.3 MCNP features

### 3.3.1 MCNP input file

The structure of input file in MCNP is shown in box 3.1. Input lines in MCNP are restricted to 80 columns and command mnemonics begin in 1-5 columns. Comment line starts with c and line after $ sign, is ignored. A continuation line starts with a space followed by & symbol and is continued till the end of the card or alternatively, with 5 blank columns [1].

Title card [one line]
Cell cards
[Blank line delimiter]
Surface cards
[Blank line delimiter]
Data cards
[Line terminator

***Box 3.1.*** *Input structure of a file in MCNP.*

The blocks corresponding to cell card, surface card and data cards will be discussed further in the following sections. Units used by MCNP are:

(i) Length in cm units

(ii) Time in shakes ($10^{-8}$ sec)

(iii) Energy in MeV

(iv) Mass density in negative g/cc

(v) Cross sections in barns ( $10^{-24}$ $cm^2$ )

### 3.3.2 Geometry specifications

MCNP treats problem geometry of an arbitrary 3-dimensional figure of a material in terms of cells or volumes bounded by surfaces. The cells are defined by the intersections, unions, and

complements of the regions [1]. Fig 3.1 shows, union operation- logical OR, which represents a region containing all area in region X and region Y. In the similar manner, Fig 3.2 shows, intersection operation- logical AND, which represents common region to both X and Y.

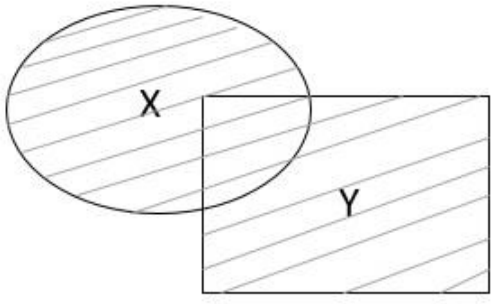


***Fig 3.1.*** *X:Y*

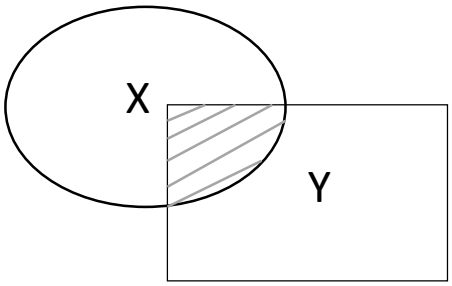


***Fig 3.2.*** *XY*

MCNP treats geometrical cells in 3-D Cartesian coordinate system. All space consists of cells or continuous regions, restricted by a surface, multiple surfaces or by infinity. There can be no gaps in the geometry that is, each point must belong to a cell or lie on the surface of cell [1].

### 3.3.3 Cell cards – block 1

Cells are defined on cells cards which is uniquely specified by a cell number, material number, and material density followed by surfaces bounding the cell. To indicate void cell, the material number and density should be zero.

### 3.3.4 Surface specifications – block 2

After defining the cells, it is necessary to describe the bounding surface of the cells. Suppose, in a problem S(x, y, z) =0 is the equation of the surface. For example, a cylinder of radius R, parallel to X axis and passing through (0, $\bar{y}$, $\bar{z}$) is given as,

$$S(x, y, z) = (y - \bar{y})^2 + (z - \bar{z})^2 - R^2 \qquad (3.1)$$

Here, mnemonic for the surface is C/X. E.g. 1 C/X 2 2 8 $ defines surface 1 as infinitely long cylinder, parallel to X axis passing through the point (y=2cm, z=2 cm) with radius 8 cm. Depending on whether or not points lie on the surface, every surface is preceded by a positive or negative sign. Any point with $S(x, y, z) > 0$ is + ve and any point with $S(x, y, z) < 0$ is − ve. For ex. a region inside the surface is positive and outside is negative. Table 3.1 gives the representation of MCNP surface cards [1].

| Mnemonics | Type | Description | Equation | Card entries |
|---|---|---|---|---|
| P | planar | General | $Ax + By + Cz - D = 0$ | A B C D |
| PX | planar | Normal to x axis | $x - D = 0$ | D |
| SO | Spherical | Centered at origin | $x^2 + y^2 + z^2 - R^2 = 0$ | R |
| S | spherical | General | $(x - \bar{x})^2 + (y - \bar{y})^2 + (z - \bar{z})^2 - R^2 = 0$ | $\bar{x}$, $\bar{y}$, $\bar{z}$,R |
| C/X | cylindrical | Parallel to X axis | $(y - \bar{y})^2 + (z - \bar{z})^2 - R^2 = 0$ | $\bar{y}$,$\bar{z}$, R |

***Table 3.1.*** *Represents MCNP surface cards.*

Fig 3.3 represents a sample surface.

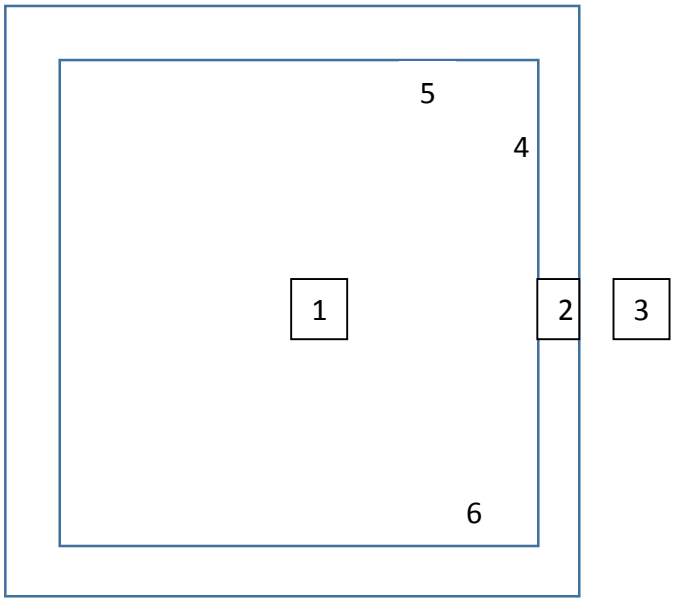


***Fig 3.3.*** A sample surface.

An example of cell card definition is 8 6 -7.86 -1 2 -3 #8 IMP: N=0 IMP: P=1

Here, cell number is the first number defined on the cell card and is randomly chosen by the user. On the cell card, second entry represents the unique material number say 6, of density 7.86 g/cc. and -1 2 -3 indicate that all space within the cell 8 is below the surface 1, above surface 2 and are below surface 3. Cell 8 defines the void region and no surface belongs to this cell. The two IMP specifications are the cell importance parameters of this region to neutrons (N) and (P) [1]. In neutron transport problem, we give neutron unit importance and photons 0

weight. Here in this cell card, we are concerned with photon transport phenomenon so it has been given unit importance.

### 3.3.4 Data specifications- block 3

This input card block gives all data specifications such as type of particles, material specification, tally score where results are to be stored, variance reduction techniques, cross section libraries, nuclear data and reactions. It doesn't provide any information regarding geometry of the surface.

#### a) Nuclear data and reactions and material specification

MCNP uses continuous energy nuclear and atomic data libraries based on evaluated nuclear data file (ENDF) system [10]. Each data file available to MCNP is listed on a directory XSDIR [2]. Specific data such as isotope composition are accessed through unique identifiers for each table, called ZAIDs, which contain A as mass number, atomic number Z, and library specifier ID [2]. For gamma ray transport, atomic number needs to be specified. For mixtures, composition should be specified by mass fraction, preceded by negative sign. For ex.
M1 83000 -0.6710 $ element Bi with Z=83 and 0.671 mass fraction in BGO crystal.

In this example, M1 represents material 1, say, bismuth with atomic number 83, followed by 000 which are place holders, required to identify specific isotopes of the element, and 0.6710 is the mass fraction of Bi in BGO crystal. MCNP can account for coherent and incoherent scattering, photoelectric absorption with the possibility of fluorescent emission, and pair production [3].

#### b) Source specification

Source description includes position, dimensions (radius) and energy of the radioactive source used in simulation. In source definition card (SDEF), MCNP allows user to specify variety of source conditions like direction, probability distributions. Analytic functions for fission and fusion energy spectra, Maxwellian, and Gaussian spectra are certain built-in functions available in MCNP.

### c) Tallies and output

There are various types of tallies permitted in MCNP, related to particle current, flux and energy deposition. The most frequently used tallies are current at a surface (F1), average flux at a surface (F2), flux at a point or ring (F5), and flux averaged over a cell (F4) [7]. Similar to flux tallies, a pulse height tally (F8 tally) provides the energy distribution of pulses created in a detector by radiation. Results are stored in the form of tallies. MCNP tallies are normalized as per starting particles. In this work, we are mostly interested in Peak Energy Deposition so we make use of F8 tally. Energy deposition starts from the source and ends when the photon is absorbed or photon is not detected if it escapes from the sample. Each tally result is printed with relative error.

### d) Error estimation in MCNP

In MCNP, tally results are printed in the output file along with relative error (R) given as, R – 1$\sigma$/estimated mean. Relative error is estimated at the end of each history. The quality of tally is determined by the range of R. Table 3.2 gives the guidelines for interpreting the value of R [2].

| Relative error | Quality of tally |
|---|---|
| 0.5 to 1 | Not meaningful |
| 0.2 to 0.5 | Factor of a few |
| 0.1 to 0.2 | questionable |
| < 0.10 | Generally reliable |
| < 0.05 | Reliable for point detectors |

***Table 3.2.*** *R value along with the quality of tally.*

The challenge in using MCNP is to minimize the computing expense required to obtain a tally estimate with acceptable relative error while performing 10 statistical checks. The 10 statistical checks are given as [1]:

- **Tally variance**: Repeating the simulation process a number of times (N), for each simulation, the variation of the mean will be distributed normally about the true mean and have a variance. This variation or uncertainty we are trying to reduce in MCNP.
- **Relation between R and N**: It follows that R decreases as N increases.
- In MCNP, acceptable value of R must be less than 10% for meaningful results.

- Relative error follows inverse sqrt N, that is, $R \cong 1/\sqrt{N}$ where N is the number of particle histories.
- **Variance of variance (VOV)** should be less than 0.1
- Variance of variance decreases with N.
- Variance of variance follows 1/N relation.
- **Figure of Merit (FOM)** = $1/R^2T$ where T is the time required for simulation and is proportional to N. N should be optimum for a specified error and least time.
- **FOM** should not be monotonically increasing or decreasing.
- Slope (Relation between R and N) should be greater than 3.

## 3.4 Modelling of detector

In the source code used to model the BGO detector, apart from the cell card definition, material description which has already been discussed in section 3.3, depending upon the source whether it is mono energetic or has multiple peaks we input the energies according to the yield percentages and then e8 tally is used for energy binning into different bins. In this work 500 bins are created with 1.5 MeV being the maximum energy. Nps includes number of histories done per second, then we use the command ip in the output to open the MCNP console for plotting and we get to see the cross sections of the detector and its surroundings. Fig 3.4 represents a typical cut away view of the modelled detector in the plane px=0 is shown below where the axis of the cylinder is along pz=0.

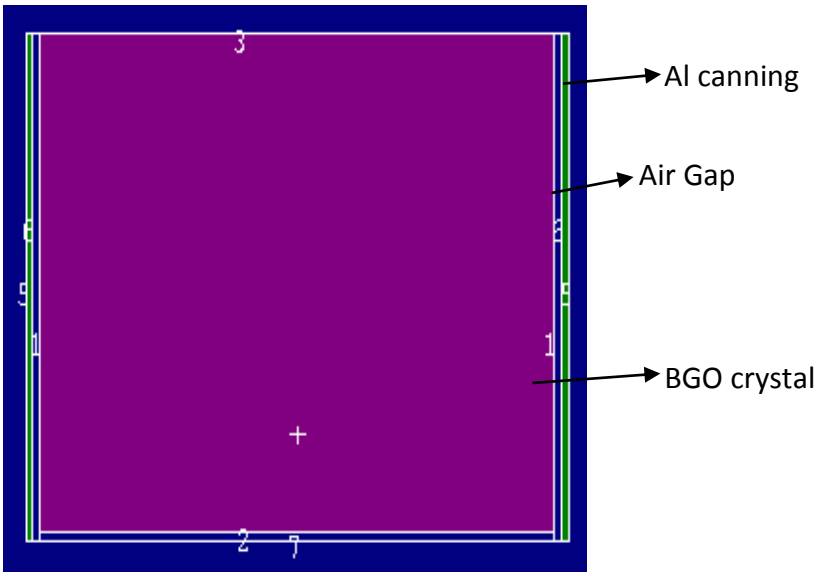


***Fig 3.4.*** *BGO modelled detector.*

We observe that the geometry of the modelled detector is in agreement with the experimental one. Effect of varying parameters such as changing source position, varying thickness of crystal have in determining the efficiency of the detector will be discussed in the later sections of this chapter.

## 3.5 Importance of Gaussian Energy Broadening factors

An ideally modelled detector will show only a single energy deposition at a particular channel and will not resemble the actual experimental spectrum, so in order to model the broadening of the peak due to detector characteristic, we make use of Gaussian Energy Broadening parameters (GEB factors). Parameters obtained using equation from experimental FWHM (Full Width Half Maximum) of the various photo peaks were used to ensure that both the spectrum match appropriately [7].

$$\mathrm{FWHM} = a + b * \sqrt{E + CE^2} \tag{3.2}$$

From the experiment, we note the FWHM values corresponding to their peak energy values of different radio nuclides. Using origin we make the best fit to account for this change. Table 3.3 represents the FWHM values corresponding to energy values of different sources.

| Energy (KeV) | FWHM (KeV) |
|---|---|
| 279 | 66 |
| 662 | 74 |
| 1332 | 100 |

**Table 3.3.** *FWHM values corresponding to gamma ray energy.*

Finally obtained values for the fitting parameters are: a= 0.04665, b=0.0276, c=0.064279.

Fig 3.5 represents the spectrum comparison with and without Gaussian energy broadening parameters.

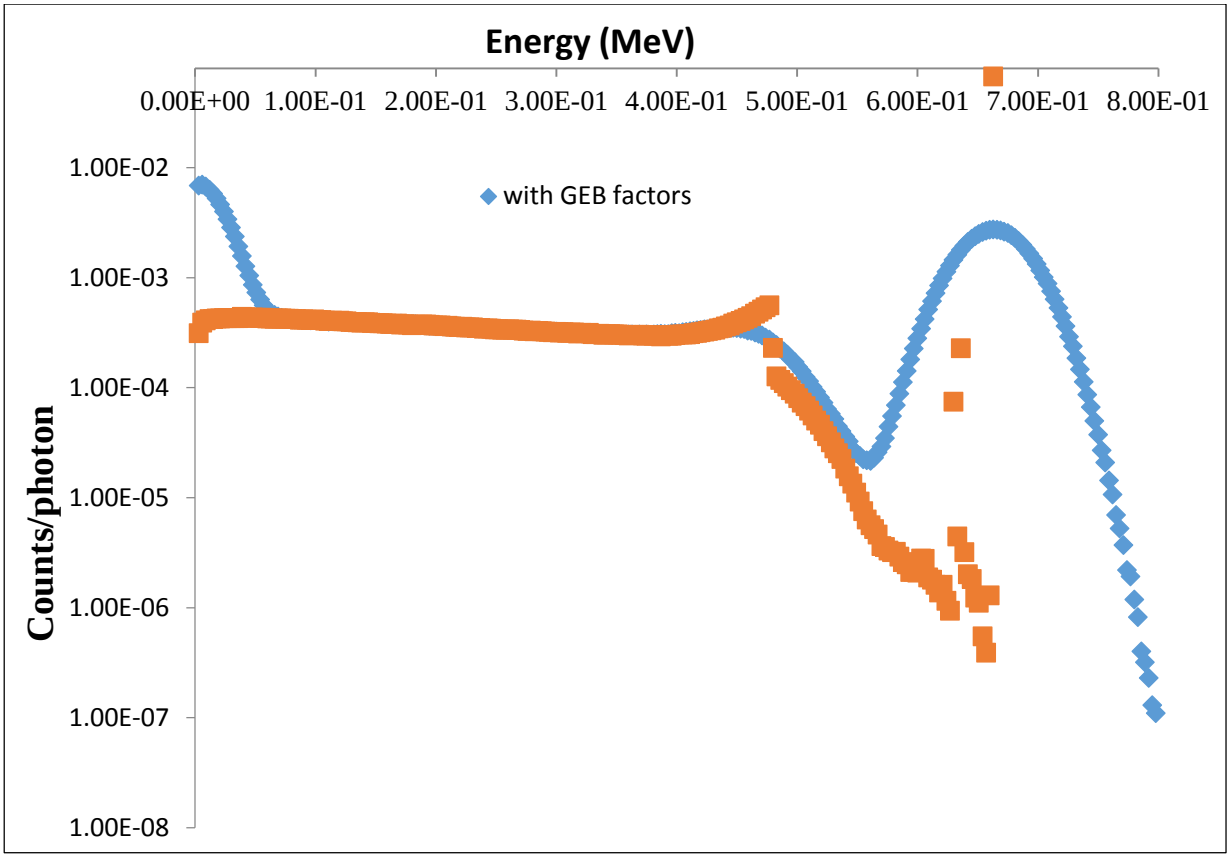


***Fig 3.5.*** *Spectrum Comparison with and without GEB parameters included. The orange and blue dotted lines represent simulation without and with GEB respectively.*

## 3.6 Simulated spectrum analysis of sources

### 3.6.1 Cesium-137 ($Cs^{137}$)

The spectrum of $Cs^{137}$ is simulated using MCNP 5 simulation, and the peak corresponds to 0.662 MeV energy. The simulated spectrum matches closely with the experimental one. Fig 3.6 shows the simulated spectrum of $Cs^{137}$.

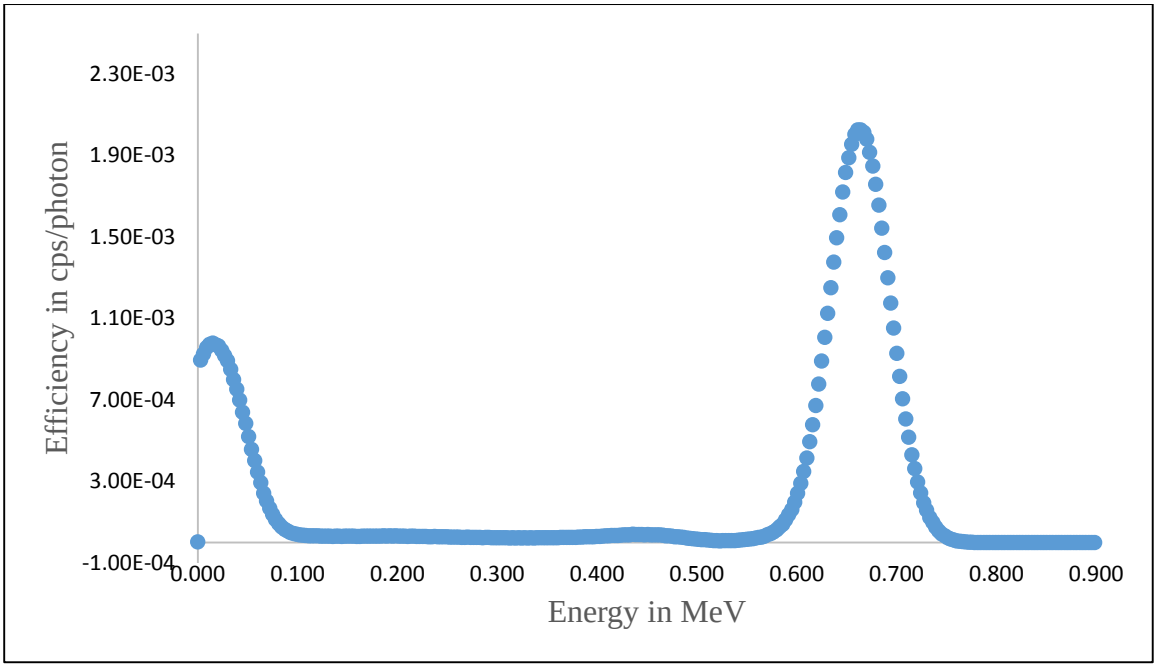


***Fig 3.6.*** *The simulated $Cs^{137}$ spectrum in BGO detector.*

### 3.6.2 Barium-133 ($Ba^{133}$)

The spectrum of $Ba^{133}$ is simulated. $Ba^{133}$ emits gamma rays of 53.7, 79.59, 81.01, 276.29, 302.71, 355.86, 383.87 keV energies [5]. The gamma yield of 81 KeV, 355.86 being 32% and 62% shows predominance over other peaks. Since in MCNP, simulation is done for 81 KeV and 356 KeV energies, the spectrum of which is shown in fig 3.7.

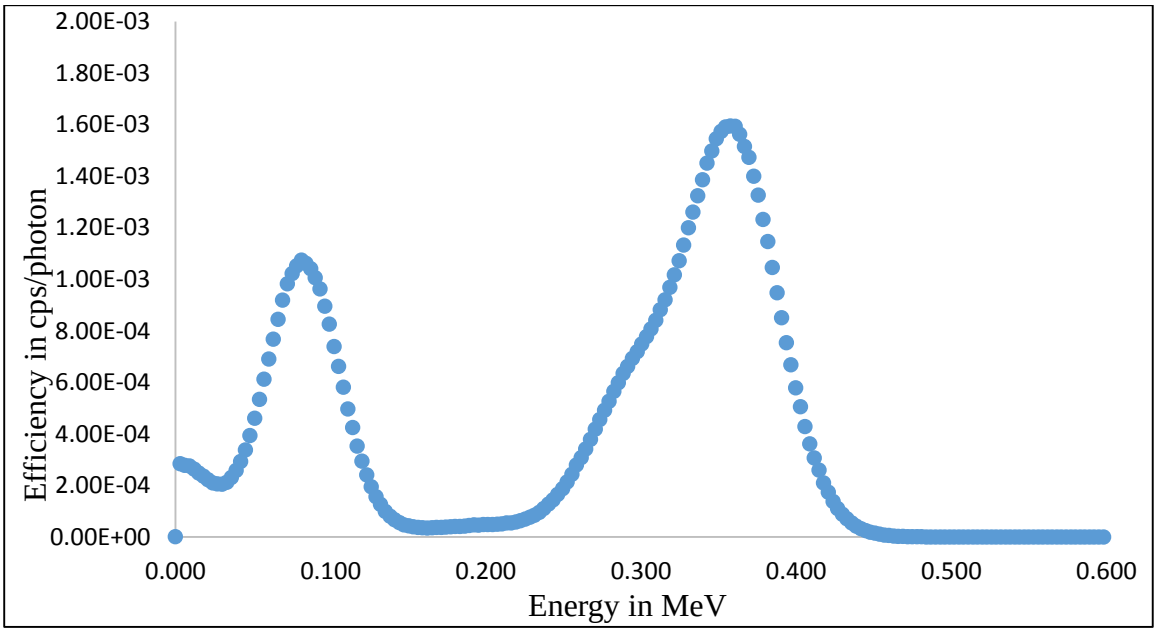


***Fig 3.7.*** *The simulated $Ba^{133}$ spectrum in BGO detector.*

### 3.6.3 Manganese-54 ($Mn^{54}$)

The spectrum of $Mn^{54}$ is simulated using MCNP 5 simulation, and the peak corresponds to 0.834 MeV energy. The simulated spectrum matches closely with the experimental one. Fig 3.8 depicts simulated spectrum of $Mn^{54}$.

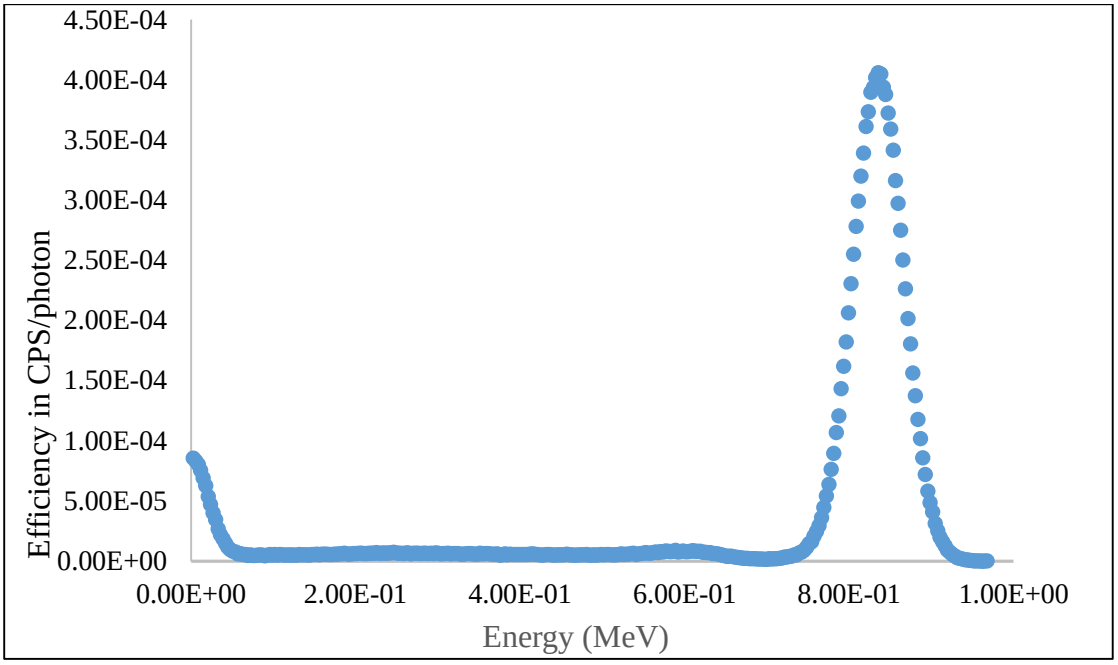


***Fig 3.8.*** *The simulated $Mn^{54}$ spectrum in BGO detector.*

### 3.6.4 Sodium-22 ($Na^{22}$)

The spectrum of $Na^{22}$ is simulated using MCNP 5 simulation, and the peak corresponds to 0.511 and 1.274 MeV energy. The source is kept at a distance of 27.2 cm from the surface of the detector. In experimental data with $Na^{22}$, a sum peak at 1.785 MeV due to 0.511 MeV and 1.274 MeV is observed. No such peak is observed in simulation. Fig 3.9 depicts simulated spectrum of $Na^{22}$.

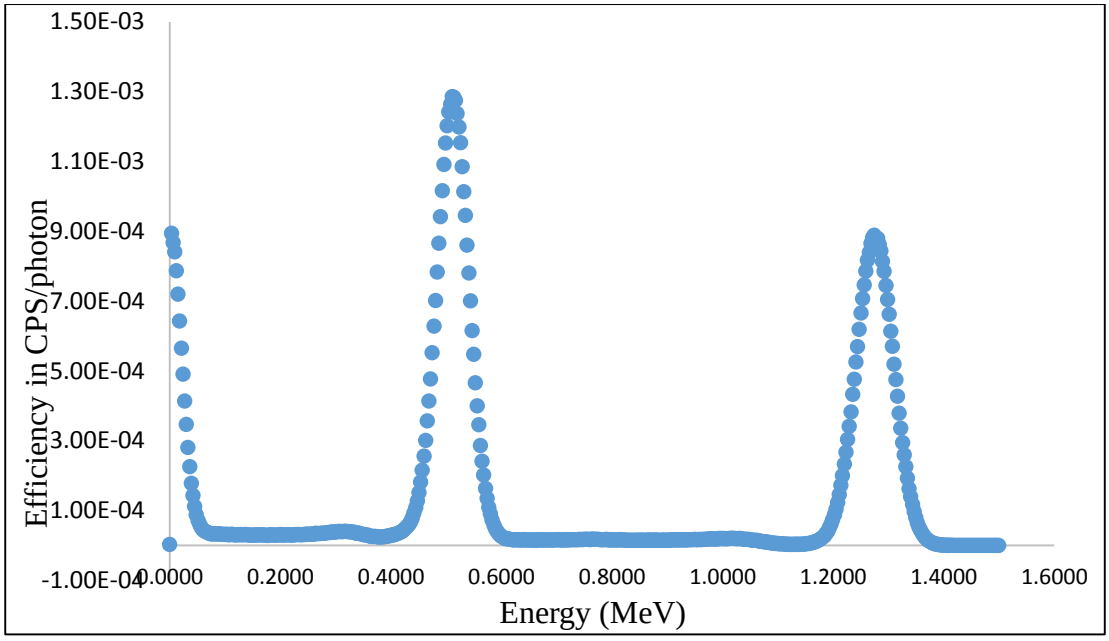


***Fig 3.9.*** *The simulated $Na^{22}$ spectrum in BGO detector.*

## 3.7 Efficiency dependence

Efficiency of a detector depends upon factors such as detector thickness, type, geometry and distance of source from the detector surface. Simulation results by varying the above parameters will be discussed in this section.

### 3.7.1 Thickness of detector surface

Taking intermediate thickness detector size in account, incident gamma ray can interact with matter through any of the processes as already discussed in section 1.2, depending on its energy. If the energy of incoming gamma ray is below 1.022 MeV, the resulting spectrum will be dominated by photoelectric absorption and Compton scattering. The narrow peak will be corresponding to photoelectric absorption known as full energy peak and continuum of energies ranging from zero to Compton edge corresponding to Compton scattering will be known as Compton continuum. There will be no contribution of Compton scattering to full energy peak.

If the incident gamma ray energy is ≥ 1.022 MeV, there is a possibility that pair production may be significant inside the detector. If one of the annihilation photon (0.511 MeV) escapes the detector, then the events lead to single escape peak at 0.511 MeV below the photo peak. If both annihilation photons escape the detector, then a peak at 1.022 MeV below the photo peak will be observed as double escape peak [3].

The source used to carry out simulations for different thickness of crystal is $Na^{24}$ and the simulated effect is as shown in the fig 3.10.

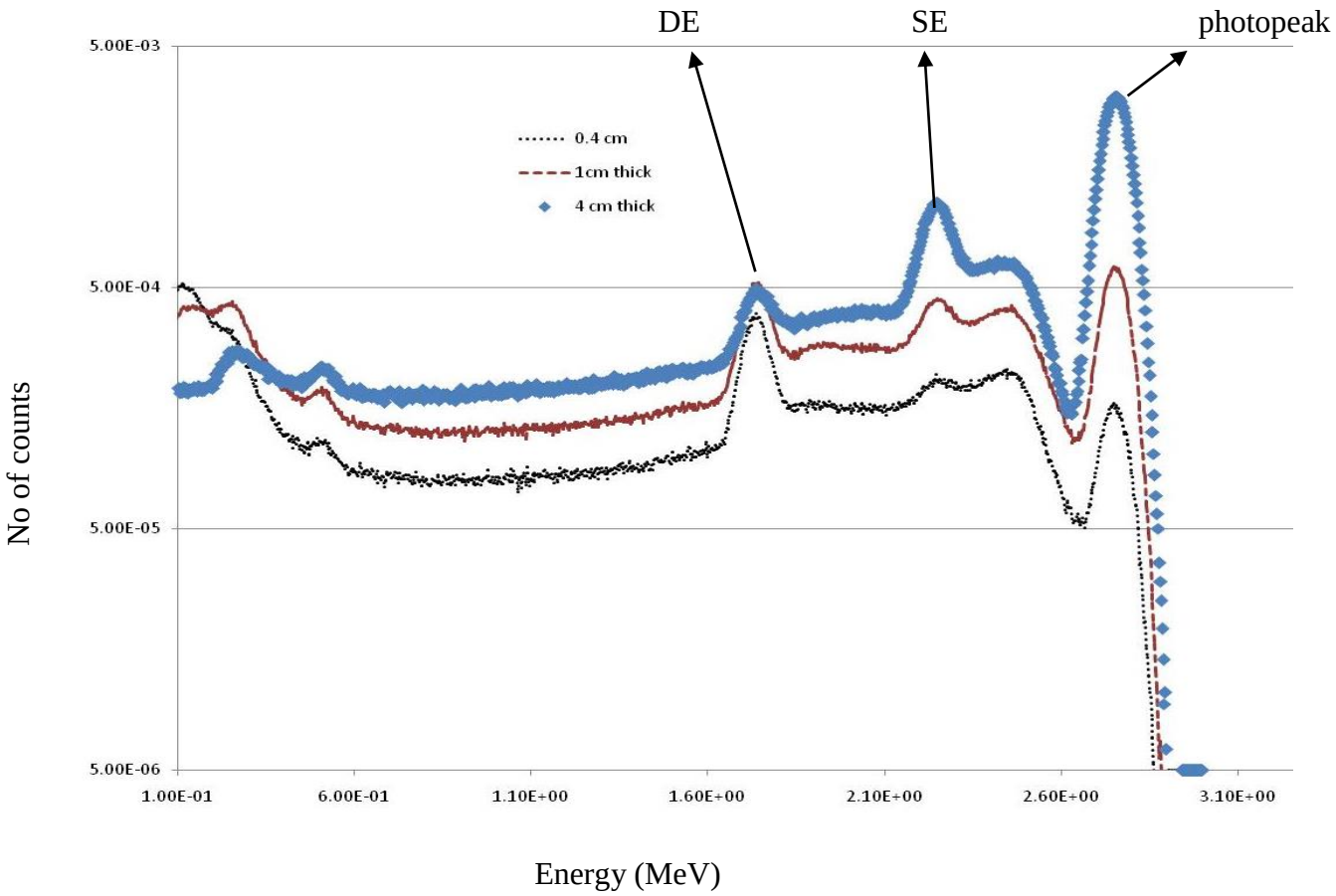


***Fig 3.10.*** *Effect of the detector thickness on the simulated spectrum. The dark blue dotted, red dotted and light blue dotted lines are for detector thickness of 0.4cm, 1cm and 4cm respectively.*

In fig 3.11 SE, refers to the single escape peak and DE refers to the double escape peak

## Inference

In this, gamma ray source $Na^{24}$, with gamma ray energy 2.754 MeV is used to study the effect of thickness. For a small detector size (0.4 cm thick), we observe that we have low intensity photo peaks and predominant single escape and double escape peaks. The single escape peak comes at [full energy peak-0.511 MeV = 2.754-0.511 = 2.243 MeV] and double escape peak at [full energy peak-1.022 MeV = 2.754-1.022 = 1.732 MeV]. On increasing the thickness of detector (1 cm thick), the height of the photo peak intensity has increased and single escape peak intensity is slightly reduced. As we go on to make the crystal thicker [4 cm], we see that photo peak intensity outweighs single and double escape peaks. Thus, the response function of the detector if thickness is varied, changes accordingly.

### 3.7.2 Effect of distance between source and detector

a) BGO with source positioned at ( 0, 0, -1.15)

The spectrum in fig 3.11 is simulated for Co-60 having gamma ray energies of 1172 KeV and 1332 KeV. The source is positioned at 1.15 cm below the detector surface, (-) sign indicates below the detector surface with x and y coordinates being 0.

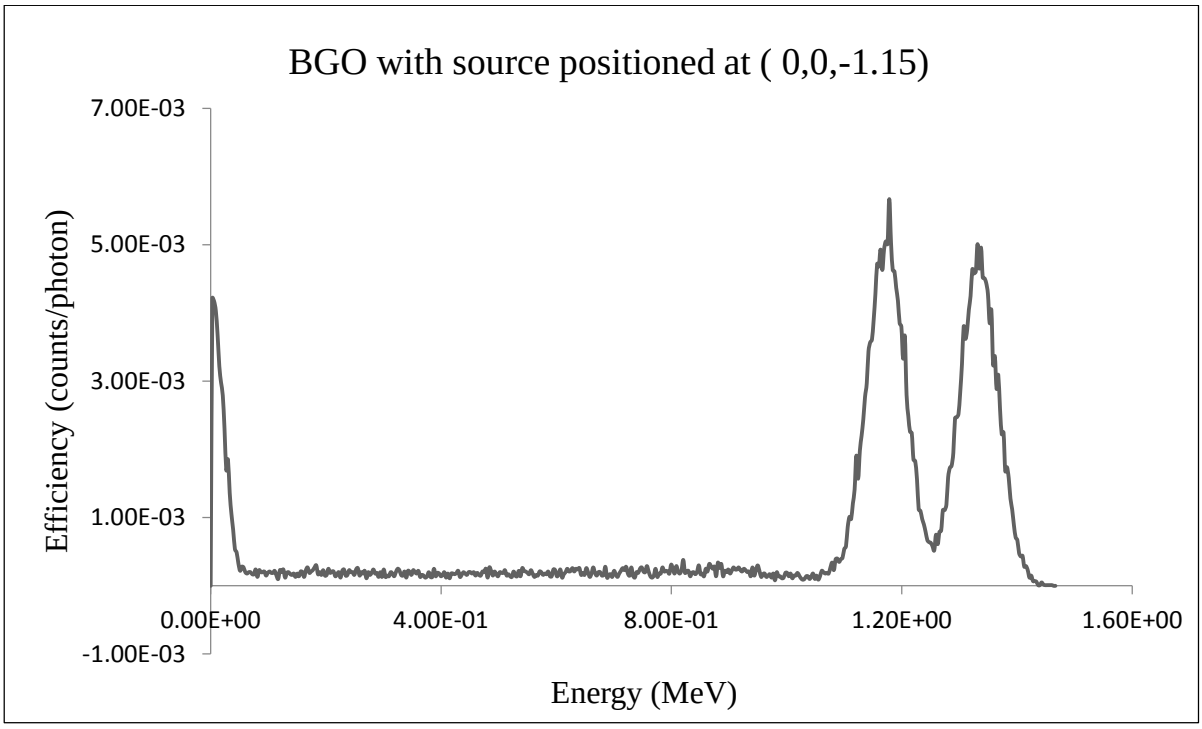


***Fig 3.11.*** *Effect of distance between source and detector when the source is positioned at 1.15 cm below the detector surface.*

b) BGO with source positioned at ( 0, 0, 11.2)

The spectrum in fig 3.12 is simulated for Co-60 having gamma ray energies of 1172 KeV and 1332 KeV. The source is positioned at 11.2 cm in front of the detector surface, (+) sign indicates above/front of the detector surface with x and y coordinates being 0.

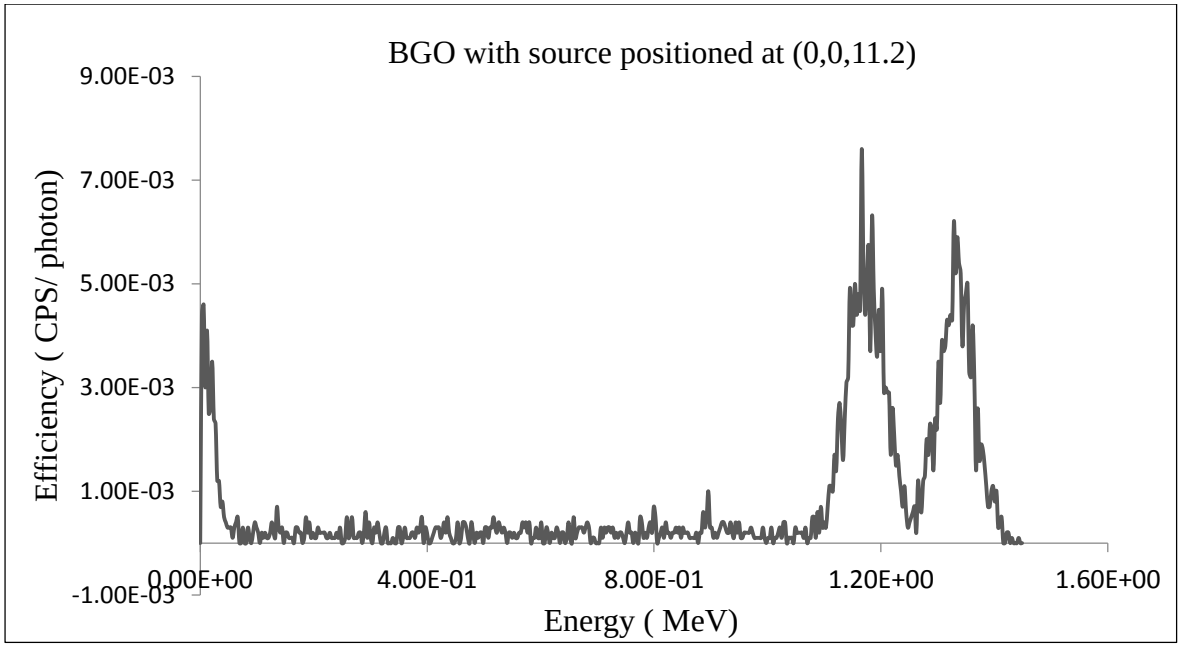


***Fig 3.12.*** *Effect of distance between source and detector when the source is positioned at 11.2 cm in front of the detector surface.*

c) BGO with source positioned at ( 0,0,7.7)

The spectrum in fig 3.13 is simulated for $Co^{60}$ when the Source is positioned at 7.7 cm in front of the detector surface, (+) sign indicates above/front of the detector surface with x and y coordinates being 0.

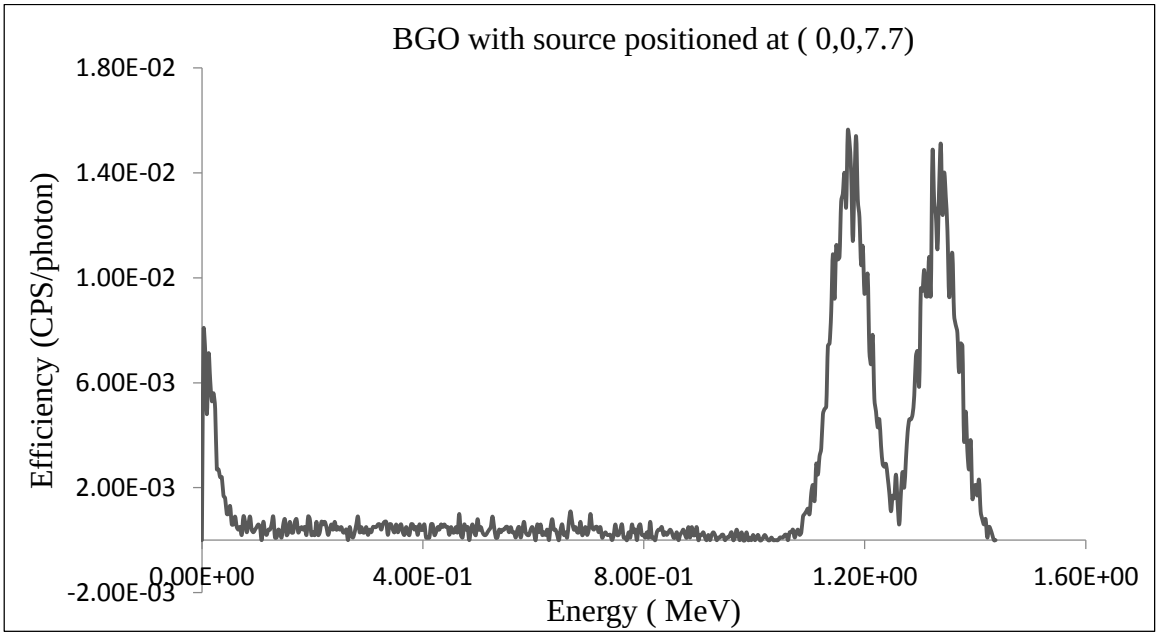


***Fig 3.13.*** *Effect of distance between source and detector when the source is positioned at 7.7 cm in front of the detector surface.*

**References:**

[1] Shultis, J. K., & Faw, R. E. (2011). An MCNP primer.

[2] Los Alamos National Laboratory (2000). MCNP4C, Monte Carlo N-Particle-transport code system

[3] Nelson, G., and D. Reilly. "Gamma-ray interactions with matter." Passive nondestructive analysis of nuclear materials (1991): 37-38.

[4]Brown, Forrest B., and Yasunobu Nagaya. "The MCNP5 random number generator." Tech. Rep. LA-UR-02-3782, Los Alamos National Laboratory, 2002.

[5] Briesmeister, Judith F. MCNP-A general Monte Carlo code for neutron and photon transport. Los Alamos National Laboratory, 1986.

[6] Briesmeister, Judith F. MCNPTM-A general Monte Carlo N-particle transport code. Version 4C, LA-13709-M, Los Alamos National Laboratory (2000)

[7] Baccouche, S., et al. "Application of the Monte Carlo method for the efficiency calibration of CsI and NaI detectors for gamma-ray measurements from terrestrial samples." Applied Radiation and Isotopes 70.1 (2012): 231

[8]Choong, W-S., et al. "Design of a facility for measuring scintillator non-proportionality." IEEE Transactions on Nuclear Science 55.3 (2008): 1756.

[9] Alghamdi, A. A., et al. "Neutron-fluence-to-dose conversion coefficients in an anthropomorphic phantom." Radiation protection dosimetry 115.1-4 (2005): 607.

# CHAPTER 4

# RESULTS AND DISCUSSIONS

The results of the experimental measurements and corresponding simulation data along with the conclusion are covered in this chapter.

## 4.1 Total efficiency comparison between the simulated and the measured spectrum for $Cs^{137}$ source

Simulated efficiency curve is plotted with exponential fit in figure 4.1. Since, we have to take in consideration the contribution of source to the obtained spectrum, we must not take into account background radiations and minor peaks from initial spectrum obtained experimentally. The major gamma ray energy peak for $Cs^{137}$ (0.662 MeV) is simulated, and a comparison between simulated and experimental efficiency value for $cs^{137}$ is established.

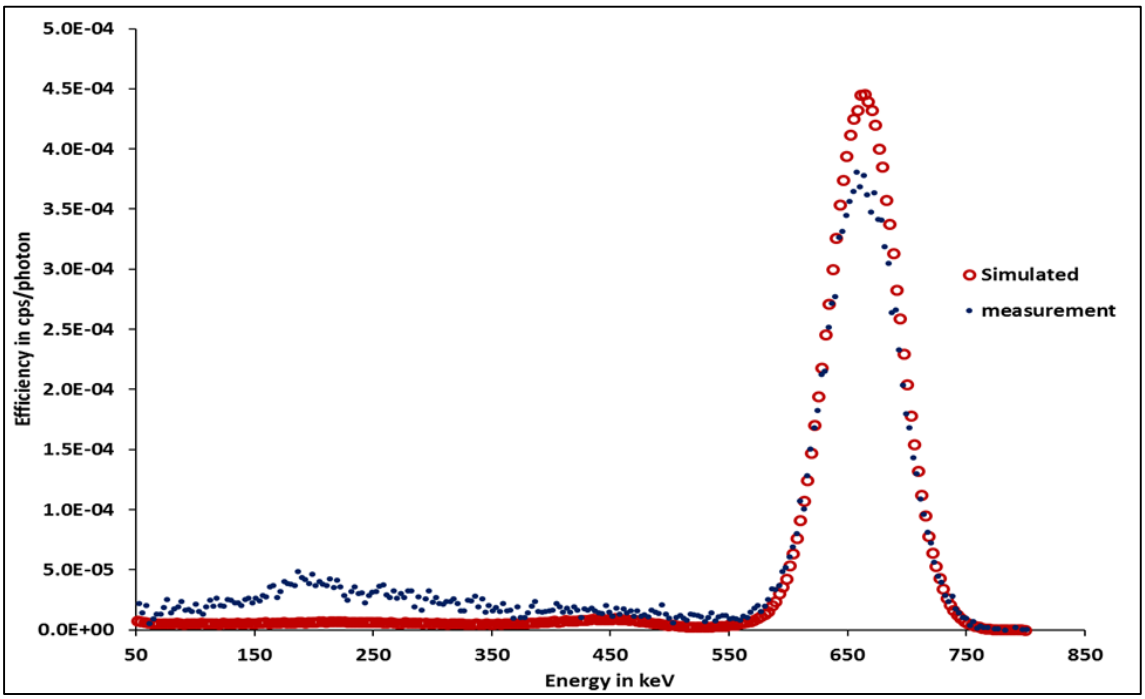


***Fig 4.1**. A comparison of simulated and experimentally measured spectra using $Cs^{137}$. The red circles and blue dotes represent simulated and experimental measurement respectively.*

## 4.2 Simulated efficiency curve of BGO detector for point source geometry

The radioactive sources were modeled as a point-like sources placed along the detector axis at a particular distance. The photon energies simulated were those belonging to the radionuclides $Mn^{54}$, $Ba^{133}$, $Cs^{137}$, $Na^{22}$ that cover the energy range of interest for measurements. The simulation of the point-like sources is used to study the variation of peak efficiency of the detector, due to change of thickness and type of canning material around the detector surface. The fig 4.2 represents the simulated efficiency curve of BGO detector for point sources.

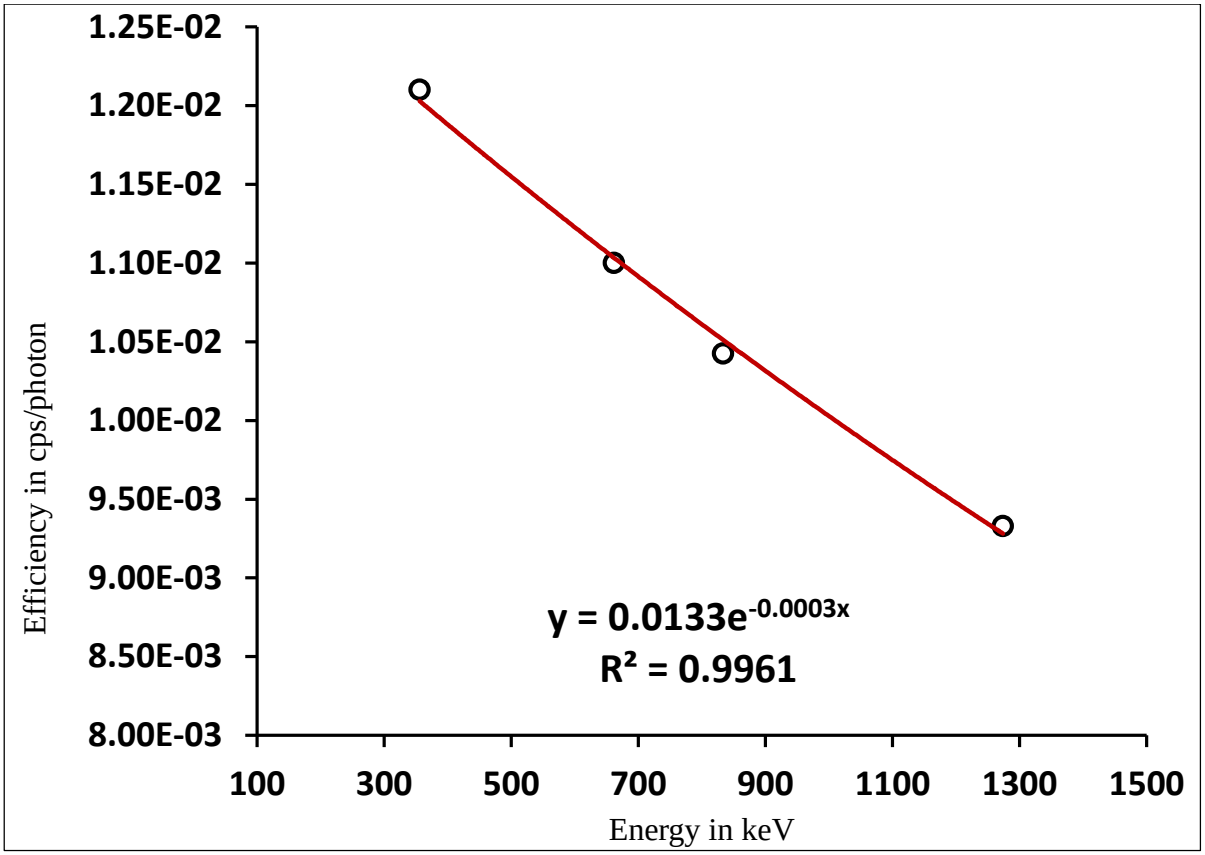


***Fig 4.2.*** *Simulated efficiency curve of BGO detector for point source geometry. The plot represents the variation of simulated efficiency of the detector with the corresponding gamma ray energy of the sources used.*

**4.3** For a $Cs^{137}$ source (662 KeV photon), if the number of histories are 1000, the relative error is found to be 3% and after increasing the number of histories to $(10)^8$ the relative error reduces to 0.09 %. Theoretically, the relative error is inversely proportional to $\sqrt{n}$. Increasing number of histories reduce the error considerably, but computation time is more in such cases.

**4.4** The deviation of simulations from experimentally calculated total efficiency for sources $Cs^{137}$, $Mn^{54}$, $Na^{22}$ results, turns to be less than 10%, as represented in table 4.1.

| Energy (KeV) | Efficiency(cps/photon) | | Deviation (%) |
|---|---|---|---|
| | Simulated | Measured | |
| 662 | 1.10E-02 | 1.03E-02 | 6.80% |
| 834 | 1.04E-02 | 9.50E-03 | 9.74% |
| 1274 | 9.33E-03 | 9.65E-03 | -3.32% |

***Table 4.1.*** *The deviation of simulated and experimentally calculated total efficiency for BGO detector.*

**4.5** As inferred from the graph 2.11, which shows the energy resolution comparison between BGO and NaI(Tl) detectors , NaI(Tl) is a better choice to detect gamma rays at low energies and BGO is fairly better choice for detecting high energy gamma rays although its energy resolution is slightly poor as compared to NaI(Tl).

## 4.6 Conclusions

- Energy calibration is carried out using BGO as a gamma spectrometer and the energy calibration factor is found to be 2.944 KeV/Channel.
- The efficiency curve is established for radioactive sources kept at 27.2 cm distance from the BGO detector surface using experiment and simulation. The comparison between measured and simulated results is worked out.
- The efficiency values for 662 KeV, 834 KeV , 1274 KeV photons, computed experimentally are compared with that of simulated values and the agreement is within $\pm 10\%$ as represented in table 4.1
- The energy resolution curve is established for BGO and NaI(Tl) detectors for radioactive sources and comparison is drawn between the two detectors. It is inferred that at high energies, BGO is a better choice to detect gamma rays.

- Total efficiency of the detector is dependent on the gamma ray energy of the source, the geometrical arrangement of the source and detector and the solid angle covered at the detector surface by source emission, It is evident from the Figs 3.12, 3.13 and 3.14 that for $Co^{60}$ as the source, the efficiency decreases with the increase in distance between

source and detector. As the distance increases from 7.7 cm to 11.2 cm with gamma emissions at normal incidence, the efficiency of the detector decreases from 0.0075 to 0.016 counts/photon. For z = -1.15 cm, the source placed at 1.15 cm below the detector surface, changes the angle of incidence with respect to detector surface, and the efficiency gets accordingly modified.